

Nathan Hugh Barr

March 30, 2019

## **Abstract**

Abstract here

# Contents

|          |   |           |
|----------|---|-----------|
| <b>1</b> | <b>Introduction</b>   | <b>3</b>  |
| 1.1      | Research Question . . . . .   | 4         |
| 1.2      | Structure of this thesis . . . . .                                    | 4         |
| <b>2</b> | <b>Theory</b>   | <b>5</b>  |
| 2.1      | Electromagnetic Radiation . . . . .                                   | 5         |
| 2.2      | Refractive index . . . . .  | 6         |
| 2.3      | Reflectance and Transmittance . . . . .                               | 7         |
| 2.4      | Fresnel equations for the ambient-substrate model . . . . .           | 8         |
| 2.5      | Fresnel equations for the ambient-thin film-substrate model . . . . . | 10        |
| 2.6      | Fresnel equations for a multilayer model . . . . .                    | 13        |
| <b>3</b> | <b>Experimental method</b>  | <b>17</b> |
| 3.1      | Polymers . . . . .  | 17        |
| 3.1.1    | Homopolymer Chemistry . . . . .                                       | 20        |
| 3.2      | Polymer Considerations . . . . .                                      | 20        |
| 3.3      | Spin Coating thin films . . . . .                                     | 20        |
| 3.4      | Spectrometer Setup . . . . .  | 22        |
| 3.5      | Reflectance measurements in the NanoCalc spectrometer . . . . .       | 23        |
| 3.6      | Reflectance measurement protocol . . . . .                            | 25        |
| 3.6.1    | Without Optics . . . . .  | 26        |
| 3.6.2    | With Optics . . . . .   | 26        |
| 3.7      | Fitting of the reflectance data . . . . .                             | 27        |
| 3.8      | Bronkhorst mass flow meters . . . . .                                 | 27        |
| 3.9      | Solvent Vapour Annealing Process . . . . .                            | 28        |
| 3.9.1    | Solvent vapour annealing protocol . . . . .                           | 29        |
| <b>4</b> | <b>Results</b>  | <b>31</b> |
| 4.1      | Light source fluctuation . . . . .                                    | 31        |
| 4.2      | Nano-Calc Simulated Reflectance Curves . . . . .                      | 34        |

|  |           |
|--|-----------|
| 4.3 Solvent vapour annealing ambient study . . . . .                 | 37        |
| 4.4 Polystyrene . . . . .  | 40        |
| 4.5 Polyisoprene . . . . .   | 41        |
| 4.6 Polystyrene-b-polyisoprene . . . . .                             | 45        |
| 4.7 Measurement table and model atble . . . . .                      | 48        |
| <b>5 Discussion</b>  | <b>50</b> |
| 5.1 Experimental setup . . . . .                                     | 50        |
| 5.2 Refractive index dispersion of polymers and absorption . . . . . | 52        |
| 5.3 Refractive index of toluene vapour . . . . .                     | 53        |
| 5.4 Mean square error fitting . . . . .                              | 53        |
| 5.5 Solvent vapour annealing . . . . .                               | 54        |
| 5.6 Polystyrene and Polyisoprene . . . . .                           | 54        |
| 5.7 Polystyrene-b-polyisoprene . . . . .                             | 55        |
| <b>6 Conclusion</b>  | <b>57</b> |
| <b>7 Bibliography</b>  | <b>58</b> |
| <b>A Fresnel functions and Dispersion files</b>                      | <b>60</b> |
| A.1 Functions . . . . .  | 60        |
| A.2 Dispersion files curves . . . . .                                | 61        |
| <b>B Scripts</b>   | <b>63</b> |
| B.1 SVA Protocol - slowslow.fps . . . . .                            | 63        |
| B.2 Light Source fluctuation study . . . . .                         | 63        |
| B.3 Nano-Calc simulated reflectance curve . . . . .                  | 64        |
| B.4 Solvent vapour annealing ambient study . . . . .                 | 68        |

# Chapter 1

## Introduction

In December 2017 and May 2018, I was asked to partake in grazing-incidence small-angle scattering(GISAXS) experiments investigating the structure of thin films at the Cornell High Energy Synchrotron Source (CHESS). A thin film is a thin layer of polymer on the nano scale deposited onto a wafer, which in this case is a silicon wafer. The experiments were conducted with the aim of understanding the reorganisation of star-block polymers on a silicon wafer, when exposed to solvent vapour annealing(SVA). The GISAXS maps are used to study how the star-block polymers arranged themselves when the polymer film swelled. The swelling dilutes the polymer, lowering its glass transition temperature, thus reducing the viscosity and increasing the chain mobility of the polymer. For diblock copolymers, swelling reduces the interfacial tension between the blocks of the diblock copolymer, and between the polymer blocks and the substrate [1]. GISAXS maps gives the researcher a snapshot of the structure of the polymer at that point in time. The GISAXS maps can be used to calculate the thickness of the polymer, but fitting a model to the data is not trivial.

This leads to the use of the experimental method called optical spectral reflectance to measure the thickness of a thin film. Using optical spectral reflectance parallel to GISAXS allows the thickness of thin films to be monitored in-situ during the solvent vapour annealing(SVA) protocols. The thickness measurements done at CHESS using optical spectral reflectance were not optimal since the software's thin film modelling and the reflectance data did not fit well. Since beam time is precious, this problem was to be investigated back at Roskilde University in between beam times.

Optical spectral reflectance is not the only experimental technique available that can measure thin film thickness; Atomic force microscopy, Ellipsometry and X-ray reflectometry can also be used. Optical spectral reflectance has been chosen to

complement GISAXS because it can be used in-situ and in harsh conditions. The size of the apparatus plays a huge role as the free space in a synchrotron hutch is limited. It is a primitive technique compared to the other techniques that use electromagnetic radiation, and it is important to investigate how far this technique can be pushed.

This thesis has two purposes. The first purpose is to describe the optical spectral reflectance experimental method and how the NanoCalc XR spectrometer and software made by the company Ocean Optics, (<https://oceanoptics.com/>) is used and how it can be optimised for the polymers used in this thesis. This will serve as an introduction to the apparatus and how light reflects and transmits through the thin film. The second purpose is to investigate how the reflectance measurements change during the solvent vapour annealing of homopolymers and diblock copolymers and if it is possible to infer the thickness of the thin films during the solvent vapour annealing.

## 1.1 Research Question

What are the advantages and limitations when using optical spectral reflectance for determining the thickness of thin polymer films during solvent vapour annealing?

What is the optimal modelling and fitting method for the optical spectral reflectance measurements and thickness determination of the homopolymers, polystyrene and polyisoprene thin films during solvent vapour annealing?

Can the same thickness determination be used on thin films with a horizontal nano scale structure such as the diblock-copolymer Polystyrene-b-Polyisoprene?

## 1.2 Structure of this thesis

The structure of this thesis is as follows. Chapter 2 will introduce the basic theory of light propagation through a vacuum and through a transparent medium. It will touch on the complex refractive index and the Fresnel equations used to model the reflectance and transmittance of light illuminating the thin films. Chapter 3 will introduce the polymers, creation of the thin films, the NanoCalc spectrometer and how the measurements are made. Chapter 4 is a collection of the results from the experiments done throughout the thesis. Chapter 5 is a discussion of the results and experiments. Chapter 6 is the conclusion of the thesis.

# Chapter 2

## Theory

The following theory is based on chapter 2 in both [2] and [3]. In this chapter, basic electromagnetic radiation theory, the definition of the complex refractive index and the definition of reflectance and transmission of light is introduced. The derivation of the Fresnel equations for multilayer thin films is introduced. The Fresnel equations are used to model the reflectance data in the analysis chapter, chapter 4.

### 2.1 Electromagnetic Radiation

Electromagnetic radiation can be expressed as a one dimensional sinusoidal wave using either cosine or sine:

$$\varphi = A \sin(\omega t - Kx + \delta), \quad (2.1)$$

where  $A$  is the wave amplitude,  $K = \frac{2\pi}{\lambda}$  is the propagation number and  $\lambda$  is the wave length, the angular frequency denoted as  $\omega = 2\pi\nu$  where  $\nu$  is the frequency,  $t$  is the time and  $\delta$  is the initial phase . From electromagnetic theory, the radiation is composed of an electric field and magnetic field that are both perpendicular to the direction of propagation. Both fields can be expressed as a one-dimensional complex sinusoidal wave. A complex number can be expressed as  $C = a + ib = Re(C) + iIm(C) = r \cos(\theta) + ir \sin(\theta)$ . Using Eulers formula  $\exp(i\theta) = \cos(\theta) + i \sin(\theta)$ , the one dimension sinusoidal wave can be expressed as:

$$\varphi = A \cos(\omega t - Kx + \delta) = Re\{A \exp[i(\omega t - Kx + \delta)]\} = A \exp[i(\omega t - Kx + \delta)]. \quad (2.2)$$

The wave travels to the right if the phase is  $(\omega t - Kx)$  and to the left if the phase is  $(\omega t + Kx)$ . Changing the order of the first two terms in the phase does not change

the propagation of the wave, only the initial phase  $\delta$ . The wave equation in equation 2.1 uses sin in the expression but the complex wave in equation 2.2 uses cosine. This is the same representation of the wave just moved  $2\pi$  in the positive direction. The electric field and magnetic field can be expressed as:

$$E = E_0 \exp[i(\omega t - Kx + \delta)] \quad (2.3)$$

$$B = B_0 \exp[i(\omega t - Kx + \delta)]. \quad (2.4)$$

The relationship between the electric field and magnetic field is given by  $E = cB$ , and can be derived using the Maxwell-Faraday equation and the one dimensional wave equations for the electric and magnetic field [4]:

$$\frac{\partial E}{\partial x} = -\frac{\partial B}{\partial t} \quad (2.5)$$

$$E = E_0 \cos(Kx - \omega t) \quad (2.6)$$

$$B = B_0 \cos(Kx - \omega t). \quad (2.7)$$

Using the Maxwell-Faraday equation the following equation can be formed:

$$\frac{\partial E}{\partial x} = -\frac{\partial B}{\partial t} \quad (2.8)$$

$$-KE_0 \sin(Kx - \omega t) = -\omega B_0 \sin(Kx - \omega t) \quad (2.9)$$

$$E_0 = \frac{\omega}{K} B_0 \quad (2.10)$$

$$E_0 = sB_0. \quad (2.11)$$

The constant  $\frac{\omega}{K}$  is expressed as the speed  $s$  of light through a medium. In vacuum the speed is equal to the speed of light  $s = c$ . Through a transparent medium, the speed is equal to the speed of light divided by the refractive index of the medium  $s = \frac{c}{n}$ .

## 2.2 Refractive index

Light travelling from one medium to another will undergo change. The speed of the light and the wavelength will change, but not the frequency. The refractive index is a material constant which describes the change and is greater than or equal to one. The refractive index is defined as:

$$n \equiv \frac{c}{s}, \quad (2.12)$$

where  $c$  is the speed of light and  $s$  is the speed of light in the medium. The amplitude of the wave will decrease in the medium because the propagation number  $K = \frac{2\pi n}{\lambda}$  increases:

$$E = E_0 \exp \left[ i \left( \omega t - \frac{2\pi n}{\lambda} x + \delta \right) \right]. \quad (2.13)$$

The change in wavelength is  $\lambda = \frac{\lambda_0}{n}$ , where  $\lambda_0$  is the wavelength before entering the medium. The medium can also absorb light, and a term is added to the refractive index to correct this. The constant  $k$  is called the extinction coefficient. The complex refractive index is given:

$$N = n - ik. \quad (2.14)$$

Placing the complex refractive index into equation 2.13, it can be seen that the amplitude of the wave will decrease exponentially.

$$E = E_0 \exp \left[ i \left( \omega t - \frac{2\pi N}{\lambda} x + \delta \right) \right] = E_0 \exp \left( -\frac{2\pi k}{\lambda} x \right) \exp \left[ i \left( \omega t - \frac{2\pi n}{\lambda} x + \delta \right) \right] \quad (2.15)$$

It needs to be stated that if the phase of the wave is expressed as  $(Kx - \omega t)$  and the complex refractive index is given by  $N = n - ik$ , the exponential factor will be positive, which is incorrect. Therefore when the phase of the wave is expressed as  $(Kx - \omega t)$ , the complex refractive index must be defined as  $N = n + ik$ .

## 2.3 Reflectance and Transmittance

When light illuminates a surface at an oblique angle, light is reflected and transmitted. The electric field of light is grouped into two oscillation directions which can be defined by two planes, the parallel plane  $p$  and the perpendicular plane  $s$ . The same applies for the magnetic field of light. The parallel plane is defined by the incident and reflected light and the perpendicular plane is perpendicular to the parallel plane. The theory of light views the two oscillation directions as the p-polarisation and s-polarisation. The reflectance of both p-polarisation and s-polarisation are defined by the ratio of the intensity of the reflected light to the incident light intensity.

$$R_p \equiv \frac{I_{r,p}}{I_{i,p}} = \frac{|E_{r,p}|^2}{|E_{i,p}|^2} = |r_p|^2 \quad R_s \equiv \frac{I_{r,s}}{I_{i,s}} = \frac{|E_{r,s}|^2}{|E_{i,s}|^2} = |r_s|^2 \quad (2.16)$$

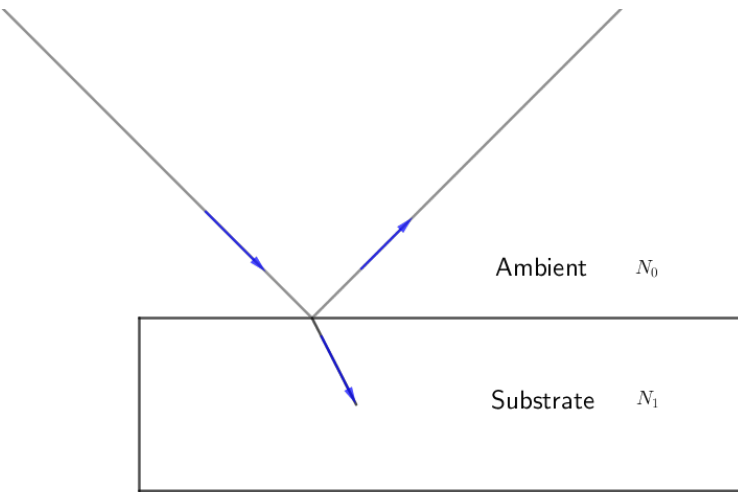


Figure 2.1: The components in this model is an ambient and a substrate both having a refractive index,  $N_0$  and  $N_1$  respectively. Light strikes the substrate reflecting with the same incident angle and refracting into the substrate. Equation 2.31 describes the amplitude reflectance coefficient of an ambient and substrate model.

The transmittance can also be expressed using the intensity ratio,  $I = N | E |^2$  and the ratio cross-sectional area for the transmitted and incident ray.

$$T_p \equiv \frac{I_{r,p} \cos(\theta_t)}{I_{i,p} \cos(\theta_i)} = \frac{N_t \cos(\theta_t)}{N_i \cos(\theta_i)} \frac{|E_{tp}|^2}{|E_{ip}|^2} = \frac{N_t \cos(\theta_t)}{N_i \cos(\theta_i)} |t_p|^2 \quad (2.17)$$

$$T_s \equiv \frac{I_{r,s} \cos(\theta_t)}{I_{i,s} \cos(\theta_i)} = \frac{N_t \cos(\theta_t)}{N_i \cos(\theta_i)} \frac{|E_{ts}|^2}{|E_{is}|^2} = \frac{N_t \cos(\theta_t)}{N_i \cos(\theta_i)} |t_s|^2 \quad (2.18)$$

$$(2.19)$$

When the extinction coefficient in the refractive index is zero,  $k = 0$ , the sum of the reflectance and transmittance is equal to one,  $R + T = 1$ . If the extinction coefficient is greater than zero,  $k > 0$ , then the sum becomes less than one  $R+T < 1$ .

## 2.4 Fresnel equations for the ambient-substrate model

Light is reflected and transmitted at the interface of the ambient and substrate as seen in figure 2.1. The boundary conditions at the interface for the electric and magnetic field in the p-polarisation can be written as:

$$E_{i,p} \cos(\theta_i) = E_{t,p} \cos(\theta_t) + E_{r,p} \cos(\theta_r) \quad (2.20)$$

$$\implies E_{t,p} \cos(\theta_t) = E_{i,p} \cos(\theta_i) - E_{r,p} \cos(\theta_r) \quad (2.21)$$

$$B_{i,p} + B_{r,p} = B_{t,p}. \quad (2.22)$$

The subscripts of the electric and magnetic field denote the incident ray  $i$ , reflected ray  $r$  and transmitted ray  $t$  in the p-polarisation  $p$  plane. The same boundary conditions for the s-polarisation can be expressed. This introduction to the Fresnel equations will use the p-polarisation light. The boundary conditions of the magnetic field need to be reformulated to express the electric field, this is done using the relation  $E = sB$ . The magnetic field boundary conditions (equation 2.22) can be expressed as:

$$\frac{E_{i,p}}{s_i} + \frac{E_{r,p}}{s_i} = \frac{E_{t,p}}{s_t} \quad (2.23)$$

$$\frac{N_i}{c}(E_{i,p} + E_{r,p}) = \frac{N_t}{c}E_{t,p} \quad (2.24)$$

$$N_i(E_{i,p} + E_{r,p}) = N_t E_{t,p}. \quad (2.25)$$

Due to the law of reflection, the angle of incidence is also the angle of reflection  $\theta_i = \theta_r$ . Placing this into the electric field boundary conditions (equation 2.21), the electric field and magnetic field can be expressed as:

$$(E_{i,p} - E_{r,p}) \cos(\theta_i) = E_{t,p} \cos(\theta_t) \quad (2.26)$$

$$\frac{N_i}{N_t}(E_{i,p} + E_{r,p}) = E_{t,p}. \quad (2.27)$$

Placing equation 2.27 into equation 2.26, the amplitude reflectance coefficient and the reflectance can be calculated for the ambient-substrate system:

$$E_{i,p} \cos(\theta_i) - E_{r,p} \cos(\theta_i) = \frac{N_i}{N_t}(E_{i,p} + E_{r,p}) \cos(\theta_t) \quad (2.28)$$

$$E_{i,p} \cos(\theta_i) - \frac{N_i}{N_t} E_{i,p} \cos(\theta_t) = \frac{N_i}{N_t} E_{r,p} \cos(\theta_t) + E_{r,p} \cos(\theta_i) \quad (2.29)$$

$$E_{i,p} (N_t \cos(\theta_i) - N_i \cos(\theta_t)) = E_{r,p} (N_i \cos(\theta_t) + N_t \cos(\theta_i)) \quad (2.30)$$

$$r_p = \frac{E_{r,p}}{E_{i,p}} = \frac{N_t \cos(\theta_i) - N_i \cos(\theta_t)}{N_i \cos(\theta_t) + N_t \cos(\theta_i)} \quad (2.31)$$

$$R_p = |r_p|^2. \quad (2.32)$$

The amplitude transmission coefficient and transmission can be equivalently formulated.

## 2.5 Fresnel equations for the ambient-thin film-substrate model

The light reflecting and transmitting in this system will interfere both constructively and destructively. To model the optical interference, the Fresnel equation for reflection will be used:

$$r_{jk,p} = \frac{N_k \cos(\theta_j) - N_j \cos(\theta_k)}{N_k \cos(\theta_j) + N_j \cos(\theta_k)} \quad (2.33)$$

The subscripts denote the reflection and transmission at a definite interface. For example  $r_{jk,p} = r_{01,p}$ , denotes the reflection at the ambient-thin film interface. In the ambient-thin film-substrate model, light at the ambient-thin film interface will be both reflected and transmitted into the layer. The transmitted ray will then be reflected and transmitted at the thin film-substrate interface. The reflected and transmitted phenomenon will proceed through-out the thin film. The change in phase at the interface is given by  $\exp(-i\beta)$ . Figure 2.2 represents the ambient-thin film-substrate model, this figure will be used to define the phase variation  $\beta$ .

The phase of the reflected ray will vary at the ambient-thin film interface. This variation can be expressed as  $K_0 \bar{AD}$ , where  $K_0 = \frac{2\pi N_0}{\lambda}$ , is the propagation number in air. The phase variation of the transmitted ray is expressed as  $K_1(\bar{AB} + \bar{BC})$ , where  $K_1 = \frac{2\pi N_1}{\lambda}$ , is the propagation number in the thin film. The length difference can be denoted as  $\bar{AB} + \bar{BC} - \bar{AD}$ , thus the phase variation of this length difference is:

$$\alpha = \frac{2\pi N_1}{\lambda}(\bar{AB} + \bar{BC}) - \frac{2\pi N_0}{\lambda}\bar{AD}. \quad (2.34)$$

Using Snells law,  $\bar{AD} = \bar{AC} \sin(\theta_0)$  and  $\bar{AC} = 2d_1 \tan(\theta_1)$  as seen from figure 2.2, this reduces  $\bar{AD}$  to:

$$\sin(\theta_0) = \frac{N_1}{N_0} \sin(\theta_1) \quad (2.35)$$

$$\bar{AD} = 2d_1 \frac{\sin(\theta_1)}{\cos(\theta_1)} \sin(\theta_0) \quad (2.36)$$

$$\implies \bar{AD} = 2d_1 \frac{\sin(\theta_1)^2}{\cos(\theta_1)} \frac{N_1}{N_0}. \quad (2.37)$$

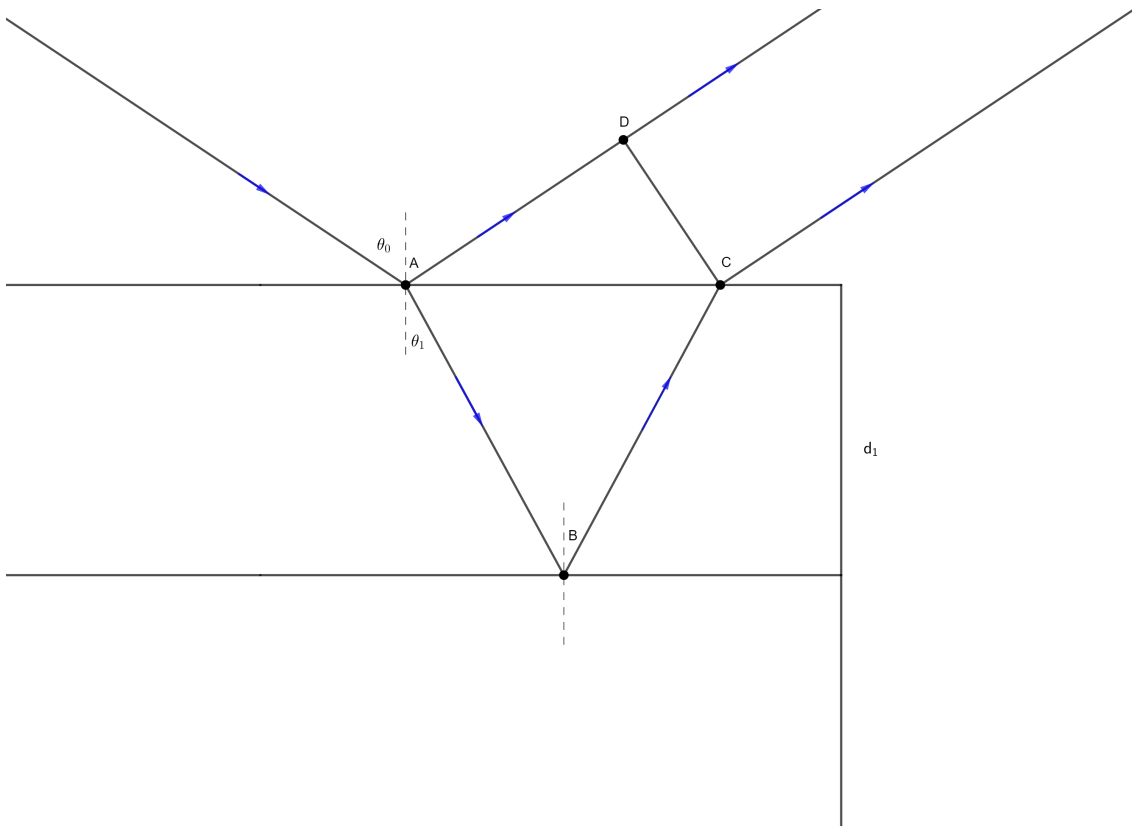


Figure 2.2: Light rays from the left will be reflected and transmitted at point A. The reflected light will experience a phase change at point A. The transmitted light will proceed to point B, where it will reflect, undergoing a phase change, then transmitting at point C. The phase difference between the primary and secondary ray can be calculated by  $\alpha = K_1(\bar{A}B + \bar{B}C) - K_0(\bar{A}D)$ .

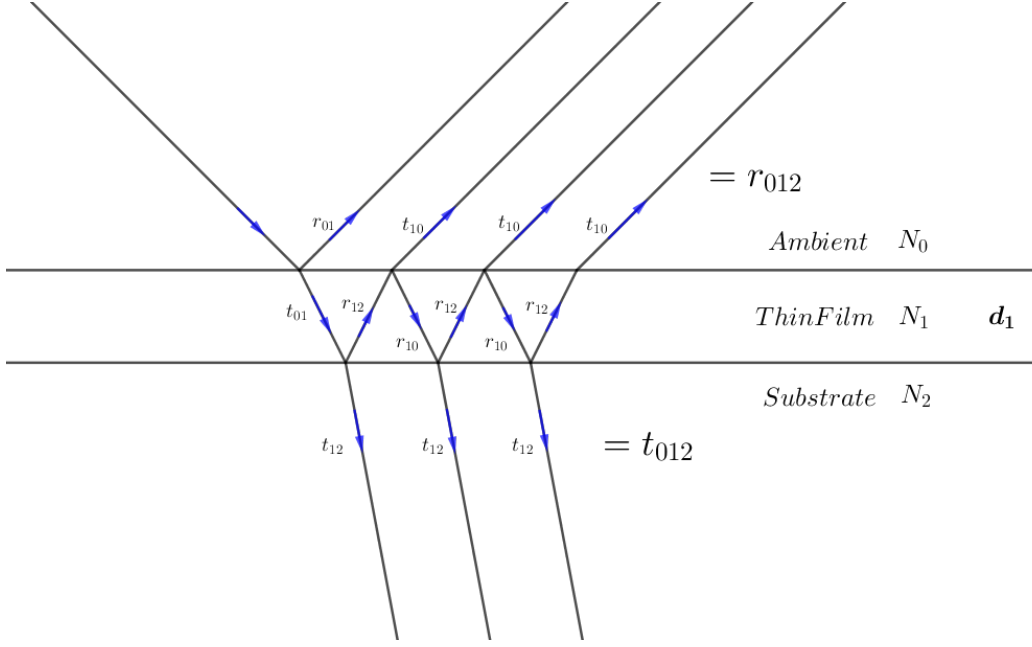


Figure 2.3: When light meets an interface, it reflects or transmits. Each light ray is named either reflection  $r$  or transmission  $t$ . Each reflected and transmitted ray is also indexed with two numbers. These denote at which interface the light was reflected or transmitted. A variation of phase happens to each reflected and transmitted ray at every interface. The phase variation at an interface can be expressed by the factor  $\exp(-i\beta)$ . The primary reflected beam is denoted as  $r_{01}$ , the second primary reflected beam is denoted  $t_{01}r_{12}t_{10}\exp(-i2\beta)$ . The reflection amplitude coefficient is the sum of reflected rays that exit the model. The transmission amplitude coefficient is the sum of the transmitted rays that continue into the substrate.

Inserting this into equation 2.34, and  $\bar{AB} = \bar{BC} = \frac{d_1}{\cos(\theta_1)}$ , as seen from figure 2.2, the equation is reduced to:

$$\alpha = \frac{2\pi N_1}{\lambda} \frac{2d_1}{\cos(\theta_1)} - \frac{2\pi N_0}{\lambda} \frac{2d_1 \sin(\theta_1)^2 N_1}{\cos(\theta_0) N_0} \quad (2.38)$$

$$= \frac{4d_1 \pi N_1}{\lambda} \left( \frac{1 - \sin(\theta_1)^2}{\cos(\theta_1)} \right) \quad (2.39)$$

$$= \frac{4d_1 \pi N_1}{\lambda} \cos(\theta_1). \quad (2.40)$$

$\alpha$  is the total phase difference of the transmitted beam, thus the expression  $\alpha = 2\beta$  must hold.  $\beta$  is called the film phase thickness and given as:

$$\beta = \frac{2\pi d_1}{\lambda} N_1 \cos(\theta_1). \quad (2.41)$$

Using figure 2.3 as a reference the amplitude reflection coefficient can be ex-

pressed as the sum of the reflected waves. The first time the ray meets the ambient-thin film interface, the ray will reflect and transmit. The reflected ray  $r_{01}$  can be calculated using equation 2.31. The transmitted ray will proceed to the next interface and reflect back to the ambient-thin film interface and transmit, giving the second reflected wave in the sum expressed as  $t_{01}r_{12}t_{10}\exp(-i2\beta)$ . The factor  $\exp(-i2\beta)$  comes from the phase difference due to the two interactions at the thin film-substrate interface and thin film-ambient interface. The phase difference factor can be collected and multiplied onto the expression since  $\varphi = A\exp(i(\omega t - (Kx + 2\beta) + \delta)) = A\exp(i(\omega t - (Kx) + \delta))\exp(-i2\beta)$ . The total amplitude reflection coefficient can be expressed:

$$r_{012} = r_{01} + t_{01}t_{10}r_{12}\exp(-i2\beta) + t_{01}t_{10}r_{10}r_{12}^2\exp(-i4\beta) + t_{01}t_{10}r_{10}^2r_{12}^3\exp(-i6\beta) + \dots \quad (2.42)$$

The amplitude reflection coefficient becomes an infinite geometric series which can be reduced using  $y = \frac{a}{(1-r)}$ , leading to the coefficient being rewritten to:

$$r_{012} = r_{01} + \frac{t_{01}t_{10}r_{12}\exp(-i2\beta)}{1 - r_{10}r_{12}\exp(-i2\beta)}. \quad (2.43)$$

The equation 2.43 can be reduced to a simpler equation using  $r_{10} = -r_{01}$  and  $t_{01}t_{10} = 1 - r_{01}^2$ :

$$r_{012} = \frac{r_{01} + r_{12}\exp(-i2\beta)}{1 + r_{01}r_{12}\exp(-i2\beta)}. \quad (2.44)$$

The following Fresnel equation, reflectance and Snell's law for this model are expressed as:

$$r_{012,p} = \frac{r_{01,p} + r_{12,p}\exp(-i2\beta)}{1 + r_{01,p}r_{12,p}\exp(-i2\beta)} \quad (2.45)$$

$$R_p = |r_{012,p}|^2 \quad R_s = |r_{012,s}|^2 \quad (2.46)$$

$$N_0 \sin(\theta_0) = N_1 \sin(\theta_1) = N_2 \sin(\theta_2). \quad (2.47)$$

## 2.6 Fresnel equations for a multilayer model

In the previous sections, the Fresnel equations for two different models were evaluated. The Fresnel equations for a multilayer model is an amalgamation of the previous models. The reflection amplitude coefficient  $r_{0123}$  cannot be calculated

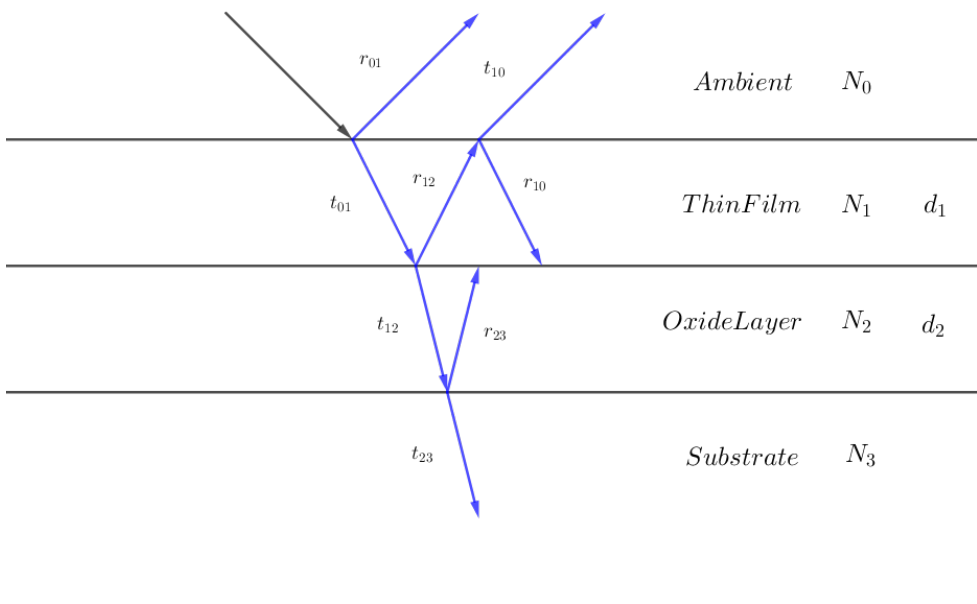


Figure 2.4: The model consists of the ambient, first thin film layer, second thin film layer and substrate. Each layer has a refractive index associated to it and both thin films have a thickness  $d_1$  and  $d_2$  respectively.

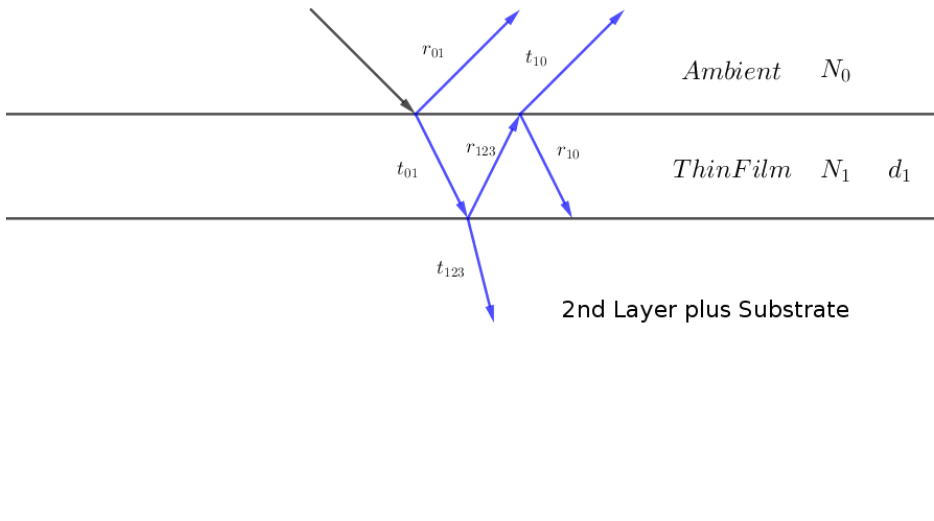


Figure 2.5: The model consists of the ambient, first thin film layer and second thin film layer plus substrate. The second thin film layer and substrate layer have been grouped together. The calculations proceed in steps. First  $r_{123}$  is calculated and then  $r_{0123}$  is calculated and summed as this figure shows. The ambient and first thin film layer have a refractive index and the first thin film layer has a thickness  $d_1$ .

in one step, the reflection amplitude coefficient  $r_{123}$  is needed first. The reflection amplitude coefficient  $r_{123}$  for the multilayer model is the two thin film layers plus the substrate. When the reflection amplitude coefficient  $r_{123}$  is calculated the substrate and the layer on top of the substrate can be grouped together and  $r_{0123}$  can be calculated. The grouping can be seen in figure 2.5. The calculations are the following:

$$r_{123} = \frac{r_{12} + r_{23} \exp(-i2\beta_2)}{1 + r_{12}r_{23} \exp(-i2\beta_2)}. \quad (2.48)$$

$\beta_2$  is the phase variation in the second thin film layer with thickness  $d_2$ . This is given as  $\beta_2 = \frac{2\pi d_2 N_2 \cos(\theta_2)}{\lambda}$ . The substrate and the layer on top of the substrate can be considered as one layer, as seen in figure 2.5, thus the reflection amplitude coefficient is expressed as:

$$r_{0123} = \frac{r_{01} + r_{123} \exp(-i2\beta_1)}{1 + r_{01}r_{123} \exp(-i2\beta_1)}. \quad (2.49)$$

The Fresnel equations have been implemented into matlab for model fitting and analysis of reflectance data. The optical fiber used in the spectral optical reflectance experiment is placed perpendicular to the thin film being measured. Thus the angle of incidence for the light is equal to zero,  $\theta = 0$ , and  $\cos(\theta) = 1$ . The incident angle can be seen in figure 2.2. The p-polarisation Fresnel equations and film phase thickness have been written into matlab as functions.

$$r_{jk} = \frac{E_r}{E_i} = \frac{N_k - N_j}{N_j + N_k} \quad (2.50)$$

$$\beta_i = \frac{2\pi d_i}{\lambda} N_i. \quad (2.51)$$

The Fresnel equations are recursive and multilayer models, and thus are easily calculated using computers. A three-layer polymer model, denoted with the subscript 1,2,3 and an ambient and substrate, denoted with the subscript 0 and 4 respectively, can be expressed as:

$$r_{01234} = \frac{r_{01} + r_{1234} \exp(-i2\beta_1)}{1 + r_{01}r_{1234} \exp(-i2\beta_1)} \quad (2.52)$$

$$r_{1234} = \frac{r_{12} + r_{234} \exp(-i2\beta_2)}{1 + r_{12}r_{234} \exp(-i2\beta_2)} \quad (2.53)$$

$$r_{234} = \frac{r_{23} + r_{34} \exp(-i2\beta_3)}{1 + r_{23}r_{34} \exp(-i2\beta_3)} \quad (2.54)$$

$$r_{jk} = \frac{N_k - N_j}{N_k + N_j} \quad (2.55)$$

The matlab functions and complex refractive indices for the silicon substrate and silicon oxide layer can be found in appendix A.

# Chapter 3

## Experimental method

In this chapter, a general outline of polymer classification will be outlined with the addition of a description of the polymers used in the solvent vapour annealing experiments. The spectrometer setup will be introduced and the necessary information related to how the spectrometer measures the reflectance of the thin films and the experimental measurement protocol will be outlined. The reflectance data fitting will be explained and the chapter will close with a brief description of the solvent vapour annealing process.

### 3.1 Polymers

Polymers are long chains of molecular units called monomers, linked together by covalent bonds. Homopolymers are polymers built of one type of monomer repeating, where diblock copolymers are built up of two types of monomers, an A monomer block and B monomer block.

Polymers can also be expressed by the degree of polymerisation,  $N$ , which characterises the average number of monomer units in the chain. It is defined as:

$$N = \frac{\bar{M}_n}{\bar{m}}, \quad (3.1)$$

where  $\bar{M}_n$  is the number average molecular weight and  $\bar{m}$  is the monomer molecular weight. The polymerisation of a diblock copolymer is the sum of the individual block polymerisation,  $N = N_A + N_B$ . The number average molecular weight is defined as:

$$\bar{M}_n = \frac{\sum N_i M_i}{\sum N_i} = \sum x_i M_i, \quad (3.2)$$

where  $x_i = \frac{N_i}{\sum N_i}$  is the fraction of the number of chains with a corresponding size range  $i$  and  $M_i$  is mean molecular weight in the size range  $i$ . The weight average

molecular weight for a polymer is defined as:

$$\bar{M}_w = \frac{\sum N_i M_i^2}{\sum N_i M_i}, \quad (3.3)$$

where  $N_i$  is the number of polymers with weight  $M_i$ . There is a dispersion of different polymer sizes in a solution, this dispersion is called the polydispersion index of the polymer and is expressed as:

$$PDI = \frac{\bar{M}_w}{\bar{M}_n}, \quad (3.4)$$

where  $\bar{M}_w$  is the weight average molecular weight and  $\bar{M}_n$  is the number average molecular weight [5].

The diblock copolymers can be further described by the volume fraction  $f$  that the different blocks take up and the Flory-Huggins interaction parameter  $\chi$  which describes the degree of incompatibility between the two polymers. The volume fraction of A and B blocks are respectively:

$$f_A = \frac{V_A}{V_{total}} \quad f_B = \frac{V_B}{V_{total}}. \quad (3.5)$$

The Flory-Huggins interaction parameter is determined experimentally and expressed as:

$$\chi(T) = \frac{\chi_H}{T} + \chi_S, \quad (3.6)$$

where  $\chi_H$  is due to enthalpy and  $\chi_S$  is due to entropy. Chemically dissimilar polymers tend to display a larger  $\chi$  value than chemically similar [6][7].

Polymers are found in different physical states, the most common being in a glass or rubber state. A glassy state is described as amorphous since the structure resembles both a liquid and a solid and this state is found below the polymers glass transition temperature  $T_g$  of the polymer. A polymer can melt into a viscous state, this state is its rubber state. This state is found above the polymers glass transition temperature [8].

Micro-phase segregation of diblock copolymers is understood as a chemical incompatibility between the different blocks in the block copolymer. The Flory-Huggins interaction parameter  $\chi_{AB}$  and the fraction composition of the copolymer  $f_A/f_B$  are used to define the morphology of the diblock copolymer. The Flory-Huggins interaction parameter describes the free-energy cost per monomer of contacts between the A and B monomers. A positive interaction parameter indicates a net repulsion between the A and B monomers, and a negative interaction parameter indicates mixing. The covalent bond plays a role in the morphology because it

prevents macro-phase separation between block A and block B of the diblock copolymer [9]. The theoretical phase diagram of a diblock copolymer is shown to the left in figure 3.1 and the experimental phase diagram for polystyrene-b-polyisoprene is shown to the right in figure 3.1. Diblock copolymers can be found in a variety of complex morphologies as seen in figure 3.1. The modelling and fitting of the homopolymers and diblock polymers will assume that the polymers are in a lamellar morphology denoted as L. The self-assembling properties of the diblock copolymers depend on the mobility of the polymer chains before structural reorganisation can proceed. This is normally done by thermal treatments above the glass transition temperature  $T_g$  of the polymer, but with high molar mass systems long annealing times are needed [10].

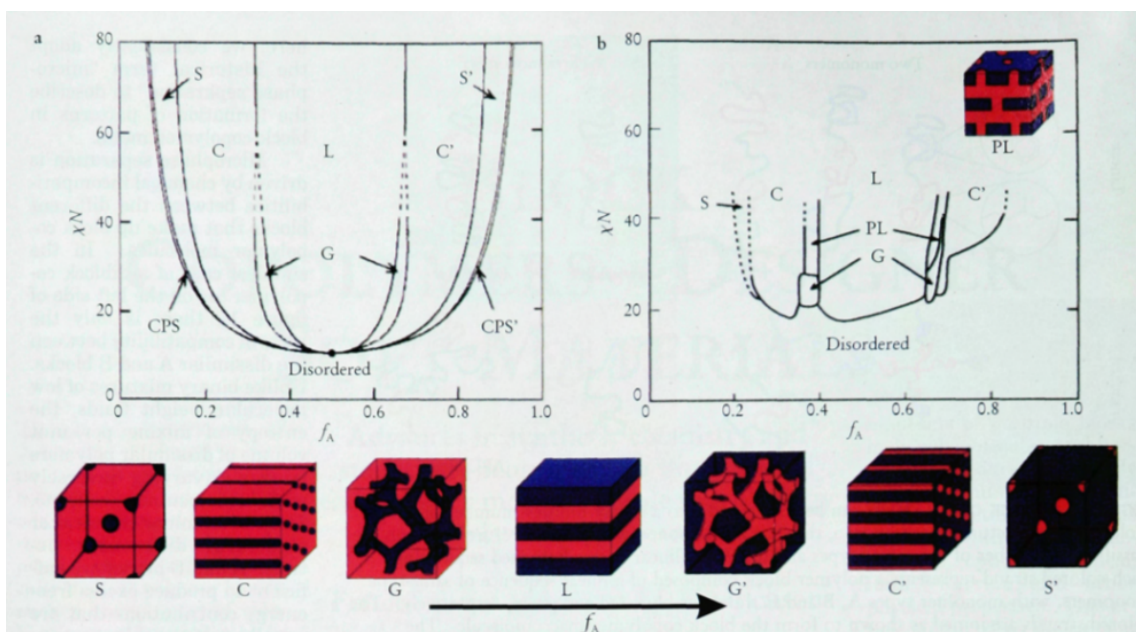
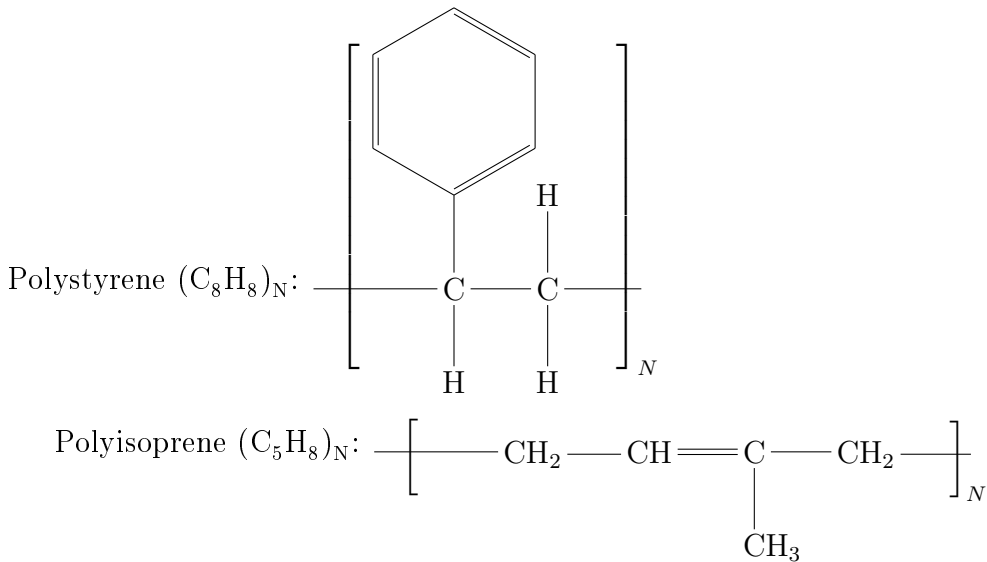


Figure 3.1: The theoretical phase diagram is shown to the left and the experimental phase diagram for polystyrene-b-polyisoprene is shown to the right. The product of the interaction parameter and the degree of polymerisation as a function of polymer composition of the A block is plotted in both figures. The morphologies the diblock copolymers can be found in are shown below the figures. From left to right the morphologies are spherical, cylindrical, gyroid, and lamellar. The experimental phase diagram for polystyrene-b-polyisoprene resembles the theoretical phase diagram. The experimental phase diagram has one extra morphology denoted as PL [9].

### 3.1.1 Homopolymer Chemistry



## 3.2 Polymer Considerations

Before commencing solvent vapour annealing some consideration is needed to determine which polymers, which solvent and which substrate should be used. Polystyrene has been chosen as block A of the block copolymer and Polyisoprene has been chosen as block B. Polystyrene is in the glassy phase at room temperature, where polyisoprene is in a rubbery phase at room temperature. The morphology of the block sheds light on how the vapour interacts with the blocks during solvent vapour annealing. The molar mass, polymerisation of both block, polydispersion index, and the interaction parameter between the two blocks is helpful in order to understand what might happen during the solvent vapour annealing process. High molar mass systems are strongly segregated and take longer to come into equilibrium than a lower molar mass system. Interaction between the solvent and the polymers will also give insight into how the morphology could evolve during the solvent vapour annealing.

## 3.3 Spin Coating thin films

Spin coating is the deposition method used to fabricate the thin films used in this thesis. This is a wet method where a polymer is dissolved in a solution, then deposited onto the semiconductor wafer, silicon wafer. The silicon wafer is rotated at a fixed low rpm to spread the polymer solution across the wafer. The rpm is increased, spinning off the excess solution and evaporation will leave a thin film with uniform thickness. This method is predicted by the following expression:

Table 3.1: Relevant values

| Polymer Values |             |              |         |
|----------------|-------------|--------------|---------|
|                | Polystyrene | Polyisoprene | PS-b-PI |
| $T_g$          | 379 K       | 204 K        |         |
| $N$            |             |              |         |
| $N_A$          |             |              |         |
| $N_B$          |             |              |         |
| $f_A$ nominal  |             |              | 0.5     |
| $f_B$ nominal  |             |              | 0.5     |
| $\bar{M}_n$    |             |              |         |
| $\bar{M}_w$    |             |              |         |
| $PDI$          |             |              |         |
| $\chi$         |             |              |         |
| $n$            | 1.60        | 1.51         | Unknown |

Table 3.2: List of polymers used in experiments

| Polymer used in experiments |              |     |                                 |  |   |
|-----------------------------|--------------|-----|---------------------------------|--|---|
| Experiment                  | Polymer      | ID  | Spincoat<br>Thickness<br>eq.3.7 | Single<br>point stage<br>static<br>thickness<br>measure-<br>ment | Single<br>point stage<br>static<br>refrac-<br>tive<br>index |
| Light Source Fluctuation    | Polystyrene  | 349 | $\approx$ 200 nm                | 280 nm   | 1.5944  |
| SVA Ambient Study           | Topsil Blank | N/A | N/A                             | N/A  | N/A   |
| Polystyrene Swelling        | PS           | 348 | $\approx$ 200 nm                | 275 nm   | 1.5975  |
| Polyisoprene Swelling       | PI           | 353 | $\approx$ 200 nm                | 301 nm   | 1.4594  |
| Polystyrene-b-Polyisoprene  | PS-b-PI      | 370 | $\approx$ 100 nm                | 97 nm  | 1.5659  |

$$d = \left( \frac{\eta}{4\pi\rho\omega^2} \right)^{\frac{1}{2}} t^{-\frac{1}{2}}, \quad (3.7)$$

where  $d$  is the predicted thickness,  $\eta$  the viscosity coefficient of the polymer solution,  $\rho$  solution density,  $\omega$  angular velocity of the spinning and  $t$  is the spinning time [8]. The spin coated block copolymers show defect-rich morphologies due to fast evaporation of the solvent and the polymers being in a thermal non-equilibrium [11].

## 3.4 Spectrometer Setup

The experimental setup is comprised of a NanoCalc XR and a Halogen light source(HL-2000-FHSA) seen in figure 3.3, which can produce wavelengths of 360 nm to 2400 nm. When the samples are being measured they are either placed on the ocean optics single point stage seen in figure 3.4 or in the solvent vapour annealing (SVA) experimental chamber seen in figure 3.5 made by the IMFUFA(Indsatsområdet for Studiet af Matematik og Fysik samt deres Funktioner i Undervisning, Forskning og Anvendelser) workshop for small angle x-ray scattering (SAXS) and grazing incidence small angle x-ray scattering(GISAXS) experiments. The NanoCalc is comprised of a spectrometer and an internal light source as seen in figure 3.6, which can produce wavelengths of 250 nm to 1050 nm and measure thicknesses of 10 nm to 100  $\mu\text{m}$ . The NanoCalc XR is connected to a computer where the NanoCalc software is installed and operated. For the experiments, the halogen light source is used since it has a larger output power than the internal light source of the NanoCalc XR. The larger intensity output is needed when performing experiments in the SVA experimental chamber. The lid of the SVA experimental chamber holds the optical fiber and light passes through a sapphire lens before entering the chamber and illuminates the thin film. The sapphire lens is needed to focus the light upon the thin film due to the distance from the optical fiber to the sample is much greater than the optimal distance of 4 mm. Throughout this thesis "with optics" will be used when referring to measurements taken using the SVA experimental chamber, since the light passes through the sapphire lens. "Without optics" refers to taking measurements using the single point stage.

For experiments done in this thesis, white light is produced by the light source(HL-2000-FHSA), which travels through optical fiber and strikes the sample. The reflected light travels back through the optical fiber and the intensity across wavelengths 400 nm-1041 nm is collected by the spectrometer and is sent to software created in-house and saved to a file and analysed in MATLAB®. Normally the

data collected by the spectrometer is analysed in the NanoCalc software but for this thesis I would like control of how the data is analysed.

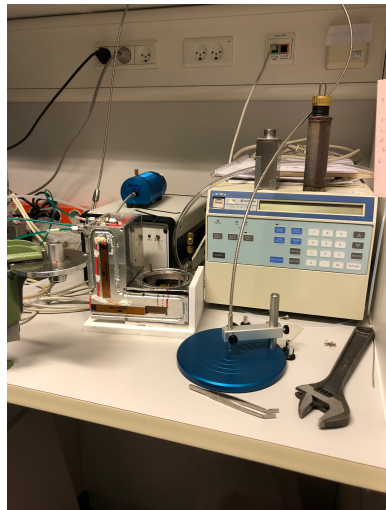


Figure 3.2: SVA experiment area

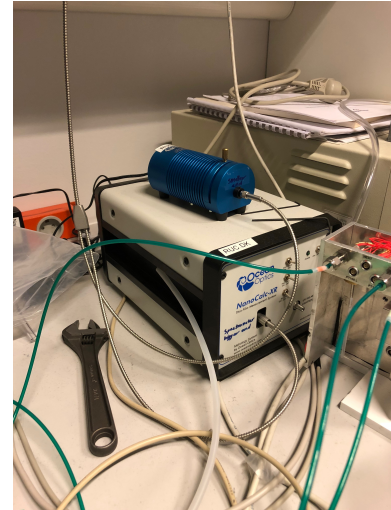


Figure 3.3: NanoCalc XR and a Halogen light source(HL-2000-FHSA)

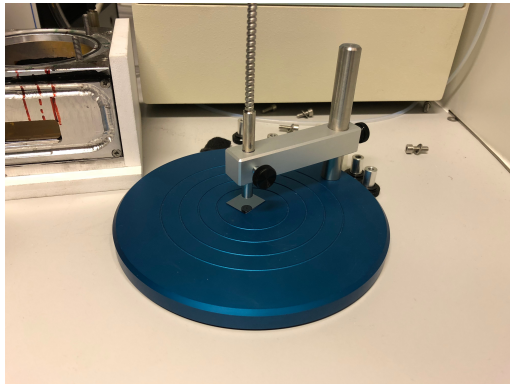


Figure 3.4: Single point stage

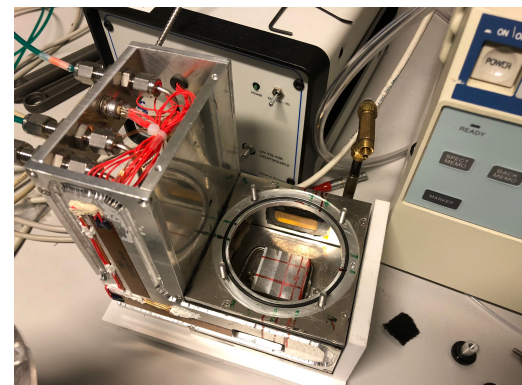


Figure 3.5: SVA experimental chamber minus lid

## 3.5 Reflectance measurements in the NanoCalc spectrometer

The NanoCalc spectrometer measures three light intensities which will be called a measurement onwards. The three measurements are the dark measurement (dark), the reference measurement (ref) and the thin-film measurement (meas). The dark measurement is the amount of stray light received by the optical fiber. The reference measurement is the amount of light reflected from a blank silicon wafer and the thin

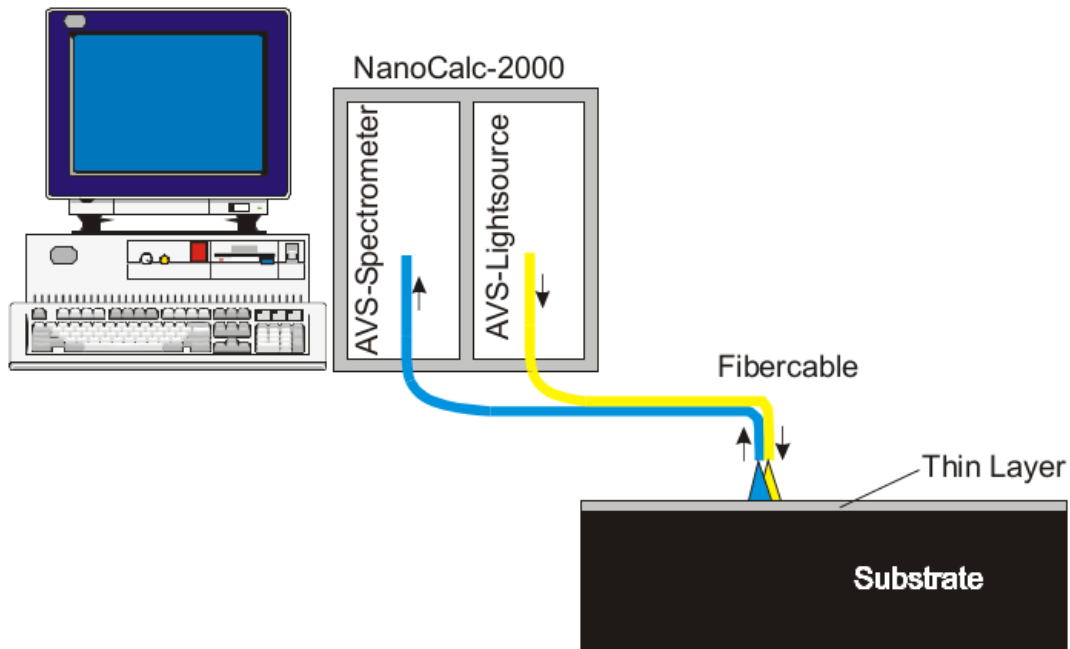


Figure 3.6: This figure describes the NanoCalc set-up and has been taken from [12]. Light from a light source travels down the optical fiber illuminating the sample. The reflected light is collected by the optical fiber and analysed in the spectrometer. The spectrometer is connected to the computer by USB and the data is sent to software created in-house and saved to a file and analysed by myself using the Fresnel equations and a fitting protocol.

film measurement is the amount of light reflected from the sample  $I_{sample}$ . From chapter 2.3, the reflectance of a sample can be expressed as :

$$R_{sample} = \frac{I_{sample}}{I_{incident}}. \quad (3.8)$$

The spectrometer does not measure the intensity of the incident light  $I_{incident}$ , therefore the reflectance of the substrate  $R_{sub}$  is used to isolate the incident light intensity and inserted into equation 3.8. The reflectance of the substrate  $R_{sub}$  is used because it can be calculated using the Fresnel equations as described in chapter 2.4.

$$R_{sub} = \frac{I_{ref}}{I_{incident}} \quad (3.9)$$

$$\implies I_{incident} = \frac{I_{ref}}{R_{sub}}. \quad (3.10)$$

Inserting equation 3.10 in equation 3.8, the reflectance for the sample is expressed without the incident light intensity as:

$$R_{sample} = \frac{I_{sample}}{I_{ref}} \cdot R_{sub}. \quad (3.11)$$

The intensities  $I_{sample}$  and  $I_{ref}$  are calculated from the meas, ref and dark. The sample intensity  $I_{sample}$  is calculated by the difference of the meas and dark,  $I_{sample} = Meas - Dark$  and the intensity  $I_{ref}$  is calculated by the difference of the ref and dark,  $I_{ref} = Ref - Dark$ . The reflectance of the sample is given as:

$$Reflectance = \frac{Meas - Dark}{Ref - Dark} \cdot R_{sub}. \quad (3.12)$$

This is the same expression given in the NanoCalc spectrometer manual [12]. Through reproduction of the data and curves given by the NanoCalc spectrometer, I can deduce that the reference measurement has already had the dark measurement subtracted, giving the following reflectance expression:

$$Reflectance = \frac{Meas - Dark}{Ref} \cdot R_{sub}. \quad (3.13)$$

Placing equation 3.13 equal to the reflectance equations using the Fresnel equations from chapters 2.4, 2.5 and 2.6, the NanoCalc spectrometer software can fit a thickness of the sample.

## 3.6 Reflectance measurement protocol

In this section, the experimental protocol for both taking measurements without the optics and with the optics are given. The halogen light source has been turned on

30 minutes prior to taking the measurements and the thin films have had 30 minutes to climatise to room temperature. The single point stage is set up and tested using a reference step wafer of known thickness. The measurement of the dark is different when using the single point stage (Without Optics) and using the solvent vapour annealing chamber (With Optics). Taking a dark measurement, without optics, is done by pointing the optical fiber away from anything that reflects. Taking a dark measurement, with optics, is done by placing a piece of dark cloth into the test chamber and taking a dark measurement with the optical fiber placed into the lid of the chamber. The protocol will be formulated in steps.

### 3.6.1 Without Optics

1. Take a continuous reference measurement and adjust the light intensity, such that the reference measurements maximum is 50% of the y-axis.
2. Clear the reference measurement.
3. Take the optic fiber and point it away from anything that can reflect light. Take a dark measurement.
4. Place the optic fiber into ocean optics single point stage. The optic fiber is positioned 4mm above the single point stage.
5. Place a blank silicon wafer under the optic fiber and take a reference measurement.
6. Save the dark and reference measurement.
7. Place a thin film on a substrate under the optical fiber and take a measurement.

### 3.6.2 With Optics

1. Take a continuous dark measurement with the optic fiber with a dark cloth in the optics where the thin film would lie, and adjust the light intensity, such that the measurement of the dark is at a maximum (100%) of the y-axis.
2. Clear the dark measurement.
3. Place a piece of dark cloth into the test chamber and place the optics into the test chamber. Take a dark measurement.
4. Remove the dark cloth and place a blank silicon wafer into the test chamber and place the optics into the test chamber. Take a reference measurement.

5. Save the dark and reference measurement.
6. Take the optics off the test chamber, remove the blank silicon wafer and place in a thin film sample. Place the optics onto the test chamber. Take a measurement.

## 3.7 Fitting of the reflectance data

The mean square error is used when fitting the Fresnel equations to the reflectance measurements. The mean square error is given by:

$$MSE = \frac{1}{n} \sum_{i=1}^n (Y_i - \hat{Y}_i)^2, \quad (3.14)$$

where  $n$  is equal to the amount of data points used,  $Y_i$  is the measured value and  $\hat{Y}_i$  is the estimated value. The fitting range is from 450 nm to 900 nm. The parameters used in the fitting of Fresnel equations are the ambient refractive index  $n_0$ , the thin film refractive index  $n_1$  and the thin film thickness  $d_1$ . The thickness for the silicon oxide layer is fixed at 2 nm and the complex refractive index values at each wavelength has been taken from Ocean Optics software. Ellipsometry measurements of the blank wafers used has fitted the silicon oxide layer to 1.7 nm. I have rounded up to 2 nm for fitting the reflectance measurements. The complex refractive index for the silicon substrate has also been taken from the Ocean Optics software. The complex refractive indices can be found in the appendix A.2. During the fitting of the results, real numbers have been used for the refractive indices for the ambient and the thin film. The fitting scripts loop through the three parameter arrays, calculating the mean square error for the measured reflectance data. The scripts find the smallest mean square error value and saves the three parameters associated to the smallest mean square error into an array. The next reflectance measurement is loaded in and the process begins again. The array is then saved into a mat file, which is read when plotting the reflectance data and fitted reflectance curves. These MSE fitting scripts can be seen in the appendix under each of the result sections.

## 3.8 Bronkhorst mass flow meters

To regulate the solvent vapour annealing process, the experimental setup includes three Bronkhorst mass flow meters. Controlling the vapour flow in different ways is important because this can have an impact in the structuring of the polymers when swelling [10]. The EL-Flow select(model name:F-201CV-500) has a flow capability

for  $N_2$  of  $4 \text{ ml min}^{-1}$  to  $750 \text{ ml min}^{-1}$ , or 400 SCCM (Standard centimetre cubed per minute at 1 atm and 273 K). The EL-Flow select(model name:F-201CV-200) has a flow capability for  $N_2$  of  $1.6 \text{ ml min}^{-1}$  to  $300 \text{ ml min}^{-1}$ , or 200 SCCM (Standard centimetre cubed per minute at 1 atm and 273 K) [13].

During both swelling processes, the SCCM will be kept constant to 200 SCCM, meaning that when the nitrogen through the chamber decreases, the nitrogen through the bubbler will increase and the total flow through the mass flow meters will add up to 200 SCCM.

## 3.9 Solvent Vapour Annealing Process

The solvent vapour annealing process is divided into two processes, a swelling and a drying process. In the swelling process a dry polymer upon a wafer is placed into the annealing chamber and is subjected to nitrogen gas. Slowly nitrogen gas is decreased and nitrogen gas through a bubbler filled with a solvent, in this thesis toluene, is increased creating vapour in the annealing chamber. When performing SVA, a solvent is chosen that is either neutral or slightly selective towards one of the polymers in the block copolymer. Solvent uptake is also dependent on the physical state of the block copolymer and the block fraction volume. The thin film will swell due to thermodynamic driving forces associated with the entropy of mixing of vapour and polymer blocks. The swelling will continue until the chemical potential of the vapour and the solvent in the thin film is in equilibrium. A diffusion front will arise continuing through the thin film from the vapour interface through to the substrate [10]. It is published that the vapour pressure is important for the thin film thickness parameter and should be controlled throughout the annealing. The vapour pressure is dependent on the temperature of the solvent and the annealing chamber. The time taken to fully swell is also dependent on how organised the dry thin film is before swelling, which leads to varying swelling time. In a solvent swollen state the mobility of the polymer chains increase and the polymer can move in the volume of the thin film. The molar mass of the polymer plays a role in how fast the polymer self-assembles and an equilibrium state may not be achieved during the swelling. In the drying step, the nitrogen gas flow through the bubbler is decreased, and the direct nitrogen gas flow is increased. The solvent in the thin film is evaporated and the rate in which the solvent evaporates has been seen to have an impact of the nanoscale structure, in the effect of quenching an organised structure. It is documented that both fast and slow evaporation leads to organised structure in block copolymers [10]. An ordering front forms in the thin film during

the evaporation where the thin films show order closer to the vapour interface and as the front propagates through the film, structural order follows in its wake[10].

Structure characterisation is important during the stages of solvent vapour annealing, and different experimental methods illuminate different parameters. Optical Spectral reflectometry used in this thesis will investigate how the thickness of the thin film evolves during SVA and shed light on how the refractive index for the ambient and thin film could evolve.

### 3.9.1 Solvent vapour annealing protocol

The solvent vapour annealing protocol used is a slow swell up to maximum toluene vapour flow which takes  $5500\text{s} \approx 92\text{min}$  and a slow deswell which is the reverse of the slow swell up to the maximum, taking  $4000\text{s} \approx 67\text{min}$  to fully dry back to roughly the start thickness. The SVA takes a total of 158 min to run and the protocol can be seen in figure 3.7. The slow swell is broken up into five regions, the first region channel 1 dry nitrogen gass (400SCCM) is set to 50% for 1000 s. In the second region, channel 1 drops to 37.5% and channel 2 which flows through the bubbler increases from 0% to 25% for 1000 s. The third region, channel 1 drops to 25% and channel 2 increases to 50% for 1000 s. The fourth region, channel 1 drops to 12.5% and channel 2 increases to 75% for 1000 s. The fifth region, channel 1 drops to 0% and channel 2 increases to its maximum 100% for 1500 s. The solvent concentration can be calculated by the solvent loading of the thin film though the volume concentration, which can be expressed using the thickness. The solvent concentration is expressed as:

$$\phi = \frac{V_{solvent+film} - V_{film}}{V_{solvent+film}} = \frac{t_{solvent+film} - t_{film}}{t_{solvent+film}} = 1 + \frac{t_{film}}{t_{solvent+film}}, \quad (3.15)$$

where  $V$  is the volume of the thin film, and  $t$  is the thickness of the thin film [14].

During the solvent vapour annealing protocol a reflectance measurement is taken every 10 seconds and saved into its own .dat file. The solvent vapour annealing protocol is controlled by a script loaded into the Bronkhorst Flowplot software. The script is called slowslow.fps and has been included in the appendix B.1 of this thesis.

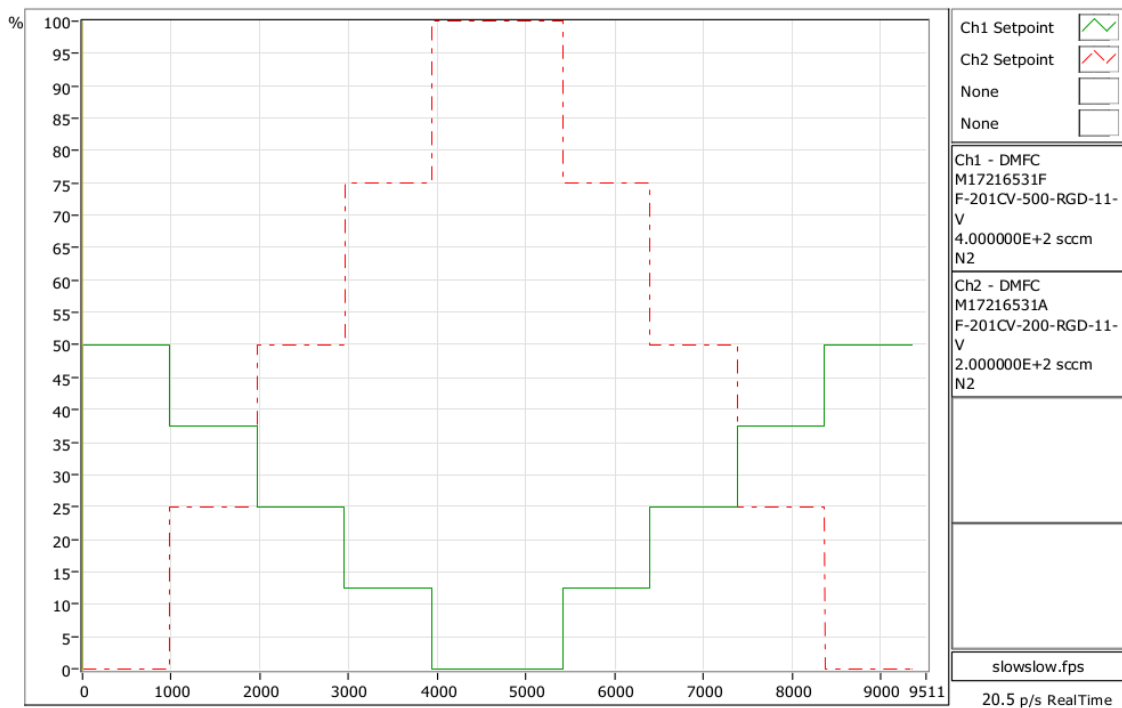


Figure 3.7: Slow swelling and slow deswelling protocol. Along the x-axis it shows the time in seconds, with the full SVA protocol taking 9500 s. Along the y-axis it shows the percentage the mass flow meters are working at. The green plot belongs to the 400SCCM Bronkhorst mass flow meter controlling the nitrogen gas and the red dashed plot belongs to the 200SCCM Bronkhorst mass flow meter controlling the nitrogen flowing through the bubbler. The swelling is done by loading a swelling script called `slowslow.fps` and this script is shown in appendix B.1.

# Chapter 4

## Results

### 4.1 Light source fluctuation

Looking at equation 3.13, which is the expression for how the spectrometer measures the reflectance of light from the thin films reveals the importance of the intensity of light being used in the measurement. A fluctuation in the intensity of light gives repercussions for both the reference measurement and the dark measurement. The measurements will be correct at the point they were taken and might not correct in future measurements. The question is how long does a reference and dark measurement remain valid? The following aims is to shed light on this problem. The scripts used can be found in appendix B.2. The thin film used is polystyrene and a total of 14 measurements were taken over a six and a half hour period. A measurement was taken every 30 min, a measurement was made manually at 10:47 and the automatic measurements commenced at 11:19. The measurements can be seen plotted together in figure 4.1. Distinguishing which curve belongs to which time is not possible because of the limited amount of plotting colours, but two groups of reflectance curves can be seen at the 600 nm mark and again at the 900 nm mark.

Figures 4.2 and 4.3 show the first reflectance measurement taken at 10:47 plotted against the reflectance measurements taken at the times 12:19, 13:49, and 15:19, 17:19 respectively. In figure 4.2, the reflectance measurements lie close to one another. In figure 4.3, the drop in reflectance seen at the 600 nm mark starts at the time 15:19 and continues onwards.

The reflectance difference has been plotted in figure 4.4. It can be seen that the difference of 10:47 plotted with both 12:19 and 13:49 lie on top of one another and the difference of 10:47 plotted with both 15:19 and 17:19 lie on top of one another. There is a clear difference between the two groups of plots.

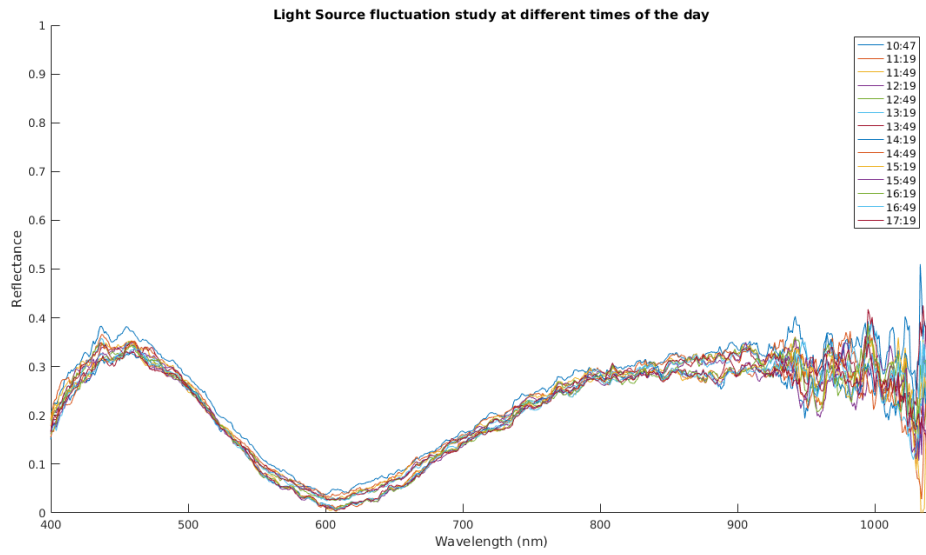


Figure 4.1: 14 reflectance measurements plotted representing a reflectance measurement taken every 30 minutes. Distinguishing which curves belongs to which time is not possible, but two groups of reflectance curves can be seen at the 600 nm mark and again at the 900 nm mark.

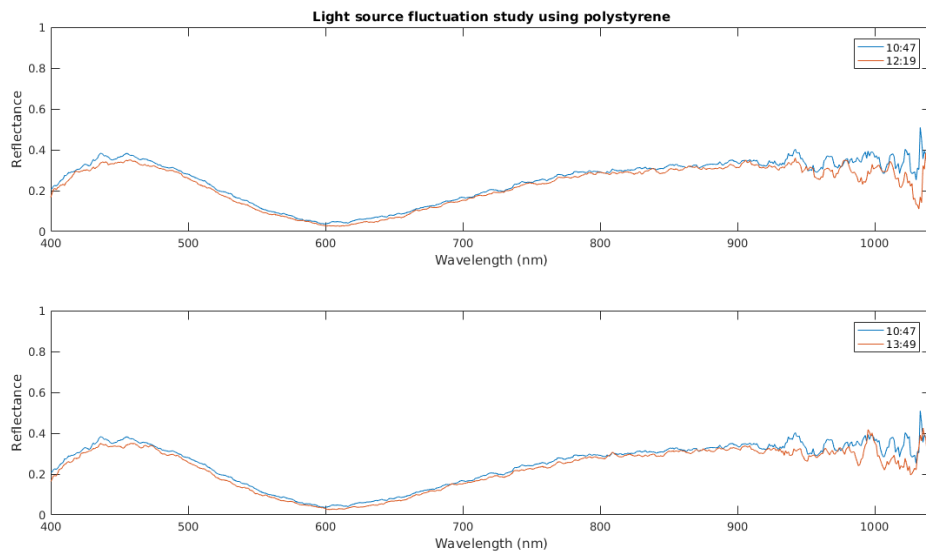


Figure 4.2: The reflectance measurement taken at 10:47 plotted with both 12:19 and 13:49. It can be seen that there is a small deviation but lay close to one another.

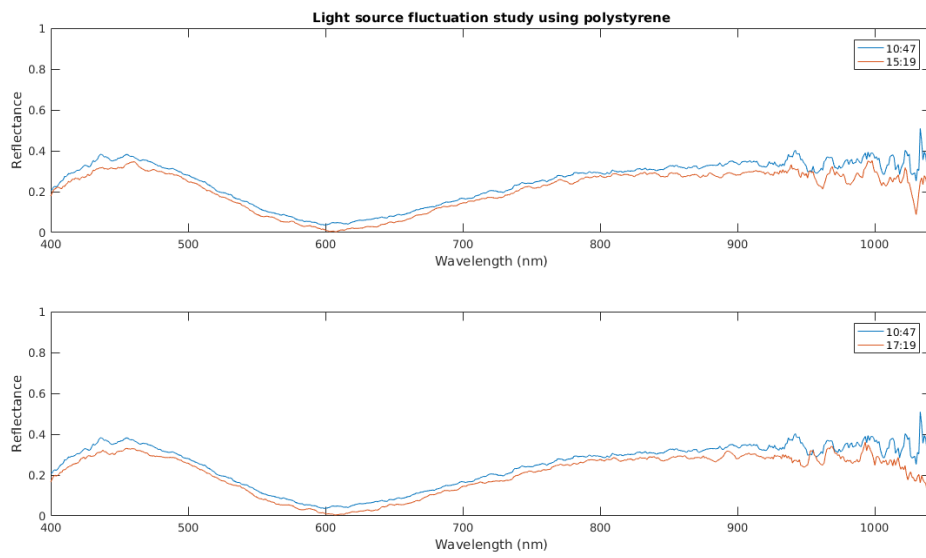


Figure 4.3: The reflectance measurement taken at 10:47 plotted with both 15:19 and 17:19. It can be seen that the deviation between the reflectance data is increasing.

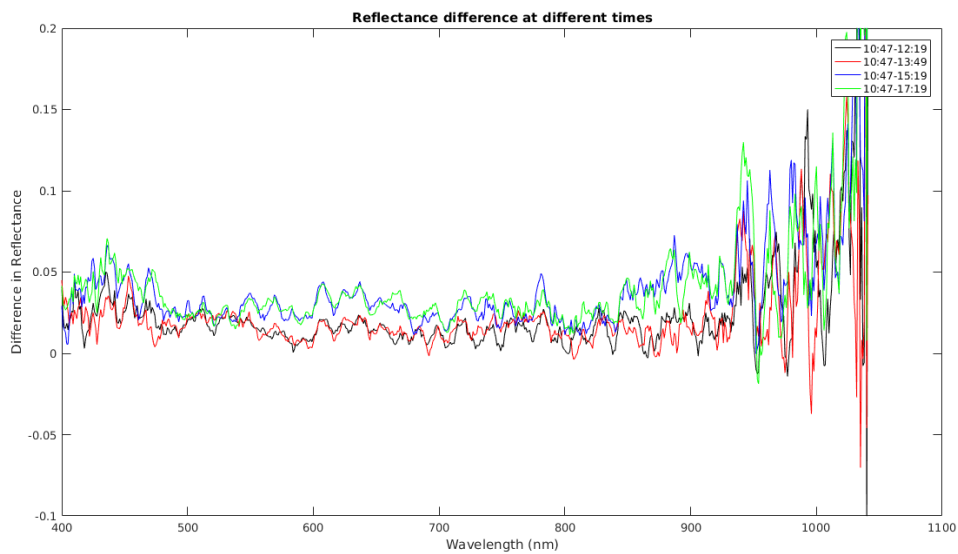


Figure 4.4: The reflectance difference between the reflectance data at 10:47 and the other times 12:19, 13:49, 15:19 and 17:19 are shown. It can be seen that the reflectance data groups itself into two, first group with times 12:19 and 13:49 and the second group 15:19, 17:19.

The conclusion to this study is that there is a 3 hour window where the variation in the intensity from the light source does not impact the reflectance measurements. Beyond the 3 hour period, the reflectance difference increases and can impact the reflectance measurements.

## 4.2 Nano-Calc Simulated Reflectance Curves

The Nano-Calc software does not go into detail how it models and analyses the reflectance curves, a little study was needed to understand the process better and test if the software uses fresnel equation and if the functions written by myself could reproduce these curves. Using the Nano-Calc software, simulated reflectance curves were produced from three models. The first model consists of an ambient consisting of air with a refractive index 1, and a silicon substrate. The fresnel equation used can be seen in equation 2.31. The reflectance curves can be seen in figure 4.6. The second model consists of an ambient consisting of air with a refractive index 1, a thin film of polymer with homogeneous refractive index 1.5 and thickness of 1000 nm and a silicon substrate. The fresnel equations used can be seen in equation 2.44. The reflectance curves can be seen in figure 4.7. The third model consists of an ambient consisting of air with a refractive index 1, a thin film of polymer using the Cauchy dispersion equation  $A = 1.4450$ ,  $B = 3 \cdot 10^4$  and  $C = 4 \cdot 10^7$ , a silicon oxide layer with a thickness of 2 nm and a silicon substrate. The cauchy dispersion coefficients have been taken from the nano-calc software and the fresnel equation used can be seen in equation 2.49 . The reflectance curves can be seen in figure 4.8. The Cauchy dispersion equation is an empirical equation describing how the refractive index varies with respect to wavelength. The Cauchy dispersion equation is defined as:

$$n(\lambda) = A + \frac{B}{\lambda^2} + \frac{C}{\lambda^4}, \quad (4.1)$$

where  $\lambda$  is the wavelength. This is the only time the Cauchy dispersion equation will be used. The coefficient A describes the refractive index when the terms with wavelength become less dominant. The Cauchy dispersion equation has not been implemented into the mean square error fitting protocol used on the reflectance data of the homopolymers and block copolymer. It is interesting nonetheless to look at the refractive index of the polymers as a function of wavelength. The cauchy dispersion equation has been plotted in figure 4.5. The coefficient have been found experimentally using ellipsometry at Thormann research group(based at Technical University of Denmark). It can be seen in figure 4.5 that polystyrene is the only

polymer which is close to a constant refractive index. Polyisoprene and polystyrene-b-polyisoprenes refractive index diverges alot compared to the constant refractive index. Since the fitting of the homopolymers and Block copolymer reflectance data is done across the interval [450 nm, 900 nm], i have included the amount in which the refractive index deviates from the constant refractive index at 450 nm in red font.

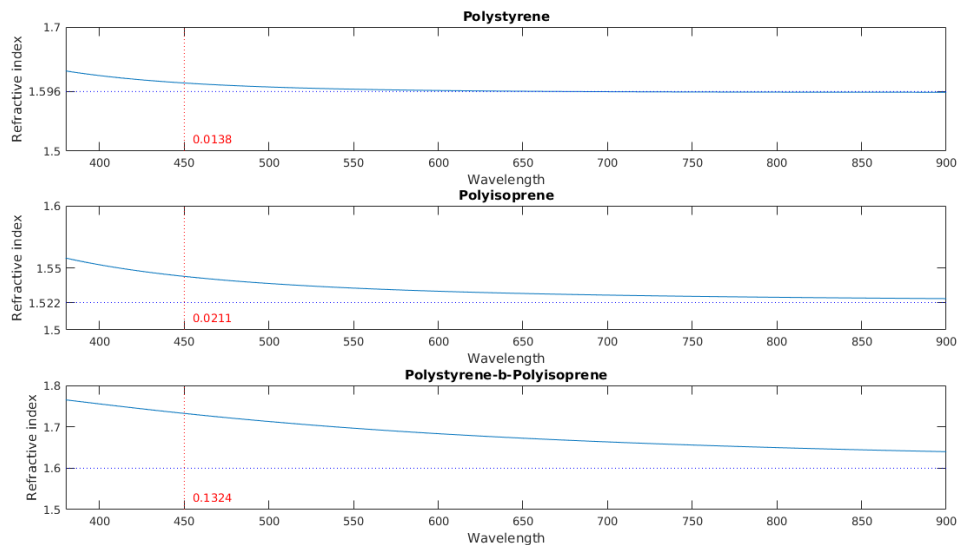


Figure 4.5: The cauchy dispersion equation has been plotted for Polystyrene, Polyisoprene and Polystyrene-b-Polyisoprene. The coefficients have been found experimentally using ellipsometry at Thormann research group(based at Technical University of Denmark), seen in table 4.1. The amount in which the refractive index deviates from the constant refractive index at 450 nm has been included in red font.

|   | Polystyrene | Polyisoprene | PS-b-PI  |
|---|-------------|--------------|----------|
| A | 1.596       | 1.522        | 1.6      |
| B | -0.0022     | 0.00203      | 0.03417  |
| C | 0.00101     | 0.00045518   | -0.00149 |

Table 4.1: Dispersion coefficients used to produce figure 4.5. The unit for B and C is squared micrometer. Wavelengths used must be in micrometers. The coefficients have been found experimentally using ellipsometry.

When modelling the Fresnel equations, both the refractive index and absorption index for the silicon oxide layer and silicon substrate have been used for the complex refractive index. The dispersion for both the silicon oxide layer and silicon substrate have been taken from the Nano-Calc software and the graphs and script to produce the graphs can be seen in appendix A.2.

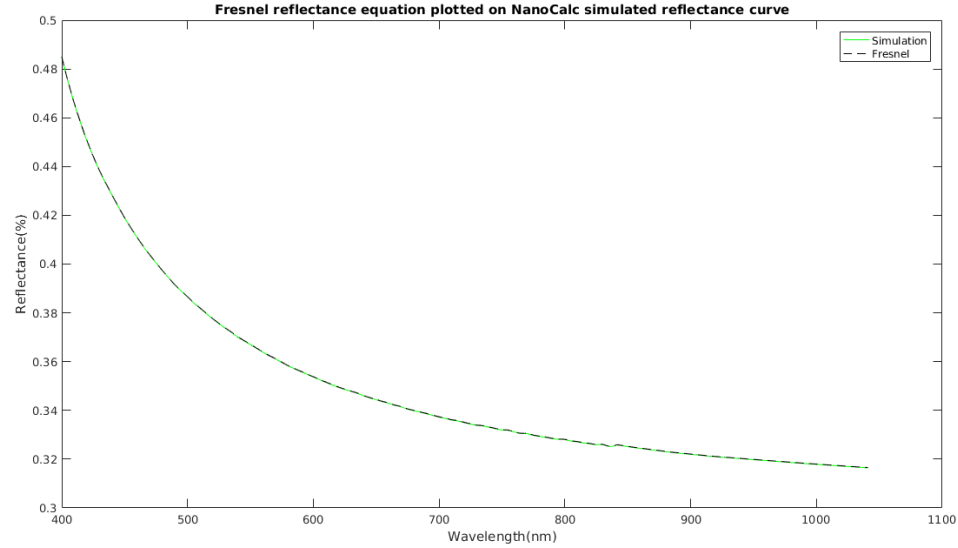


Figure 4.6: Simulated curve of the model plotted with the green curve, consists of ambient of air refractive index 1, and the silicon substrate. The Fresnel equations plotted with the black dashed curve consists of the same model. It can be seen that the two curves fall upon each other.

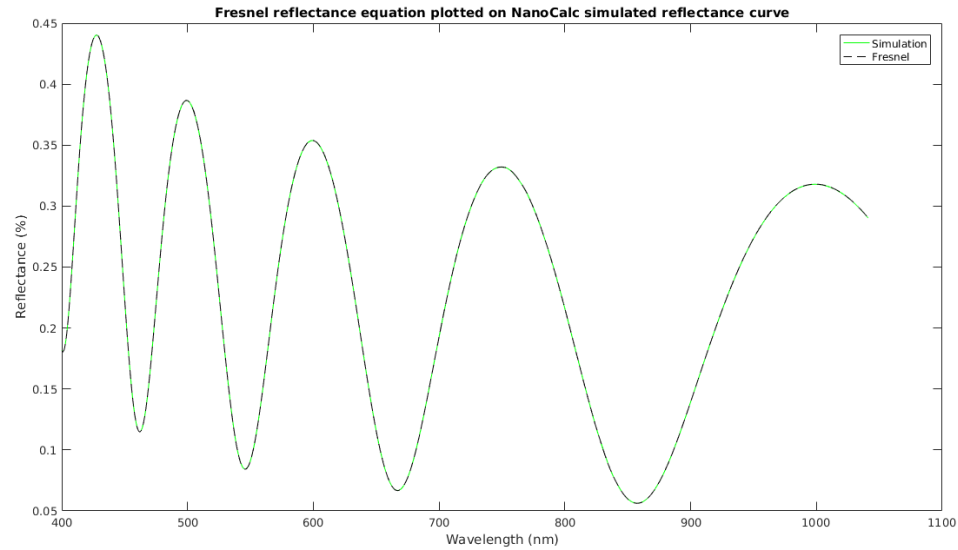


Figure 4.7: Simulated curve of the model plotted with the green curve, consists of ambient of air refractive index 1, a thin film of polymer with homogeneous refractive index 1.5 and thickness 1000 nm and the silicon substrate. The Fresnel equations plotted with the black dashed curve consists of the same model. It can be seen that the two curves fall upon each other.

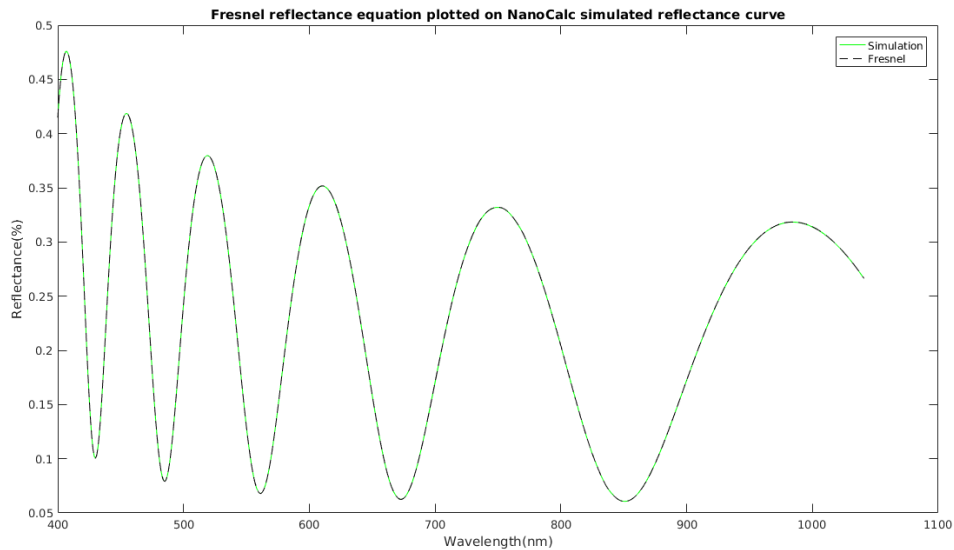


Figure 4.8: Simulated curve of the model plotted with the green curve, consists of ambient of air refractive index 1, a thin film of polymer using the Cauchy dispersion equation  $A = 1.4450$ ,  $B = 3 \cdot 10^4$  and  $C = 4 \cdot 10^7$ , a silicon oxide layer with thickness 2 nm and the silicon substrate. The Fresnel equations plotted with the black dashed curve consists of the same model. It can be seen that the two curves fall upon each other.

Two conclusions have been drawn from this study. The first is that the Fresnel equations implemented by myself in the script used in this chapter can reproduce the simulated curves used by the Nano-Calc software to model the reflectance curves. The second is that the mean square error fitting protocol for fitting the reflectance data will not implement a cauchy dispersion for refractive index because adding three new parameters to fit to will increase the fitting time dramatically.

### 4.3 Solvent vapour annealing ambient study

During solvent vapour annealing, nitrogen flow through the bubbler increases, increasing the toluene vapour present in the chamber. The question arises, does the refractive index of the ambient increase with the increase of toluene vapour available in the chamber? A blank silicon wafer has been used for this study. Upon the silicon wafer lies a silicon oxide layer modelled to have a thickness of 2 nm. The refractive index has been allowed to vary between 1 through to 2 with a step of 0.1. The fitting protocol loops through each refractive index, calculating the theoretical reflectance curve from the fresnel equation 2.31. The mean square error has been calculated for each loop and the minimum has been found and the refractive index

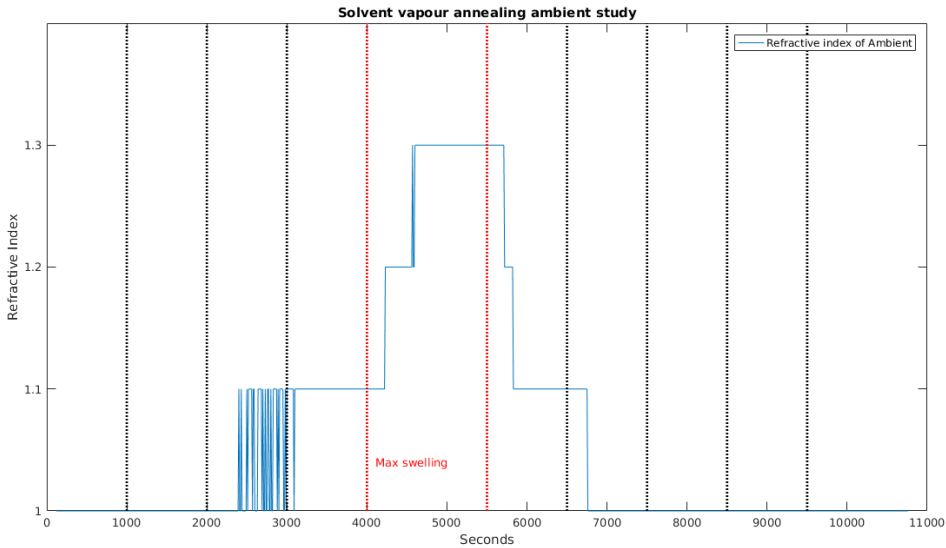


Figure 4.9: The refractive index of the ambient has been plotted. The refractive index values have been found by using the mean square error fitting protocol. The refractive index from the lowest mean square error has been used per reflectance measurement. The dotted vertical lines represent the swelling and deswelling step outlines in section 3.9.1. The red dotted lines indicate the period where there is maximum flow through the bubbler.

saved into a file. The swelling protocol used has been outlined in section 3.9.1 and can be seen in figure 3.7. From the mean square error fitting, the refractive index varied between 1 through to 1.3 through the course of swelling, this can be seen in figure 4.9. The dotted vertical line represent the different stages in the solvent vapour annealing and the maximum flow through the bubbler has been highlighted with the red vertical dots.

The mean square error for each reflectance measurement is shown in figure 4.10. It can be seen between the 2000 and 3000 second mark the refractive index is erratic, this is mirrored in the increase in the mean square error. The same happens when the fitting increases the refractive index to 1.3, the mean square error increase then falls. During the deswelling period there is an increase in mean square error when ever the refractive index decreases. When watching the reflectance data play like a movie, it can be seen that the reflectance does decrease. The decrease in reflectance data is shown in figure 4.11. As stated the wafer used is a silicon wafer with an oxide layer. In the modelling the oxide layers thickness is fixed to 2 nm. Both layer are unable to take up vapour and their thicknesses cannot increase, thus the variable that can vary is the ambient refractive index.

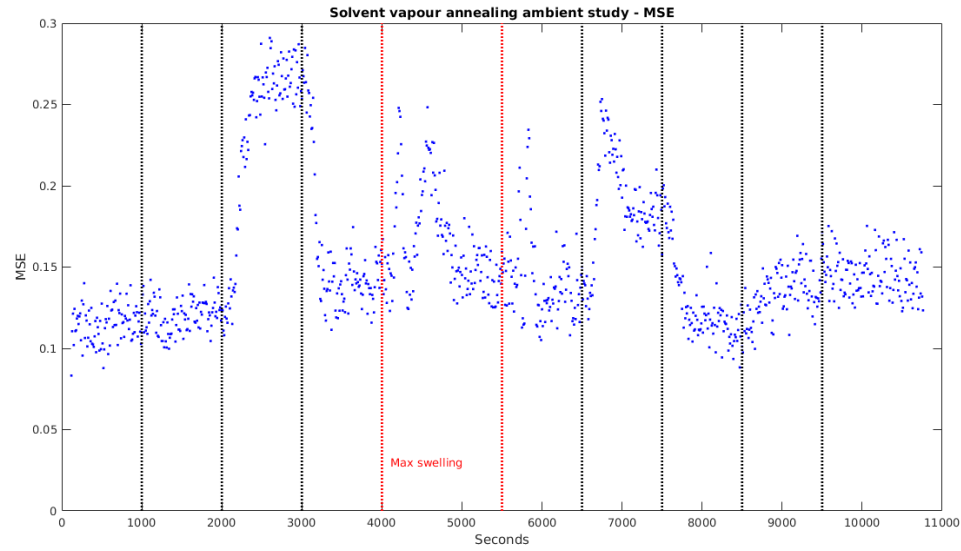


Figure 4.10: The mean square error has been plotted as a function of time. The frames have been captured every 10 time. It can be seen that the error increase every time the modelling increases or decreases the refractive index but stabilises back to a level close error before the change in refractive index.

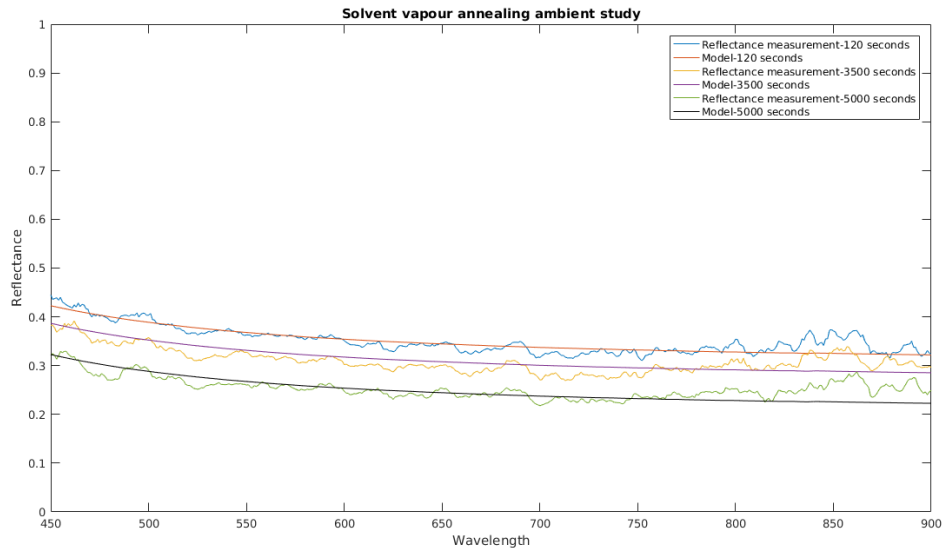


Figure 4.11: Three reflectance curves has been plotted to show how the reflectance decreases during solvent vapour annealing when the toluene vapour in the chamber increases. The fresnel reflectance model equation 2.31 has been plotted for each stage in the solvent vapour annealing. The measurement at time 120 second is modelled with a refractive index of 1. The measurement at time 3500 time is modelled with a refractive index of 1.1. The third measurement at time 5000 time is modelled with a refractive index of 1.3.

The conclusion to this study is that the ambient in the solvent vapour annealing chamber increase during the swelling. The interval in which the refractive index of the ambient increase, lies between 1 and 1.3.

## 4.4 Polystyrene

Polystyrene with a measured thickness of 275.5 nm and a refractive index 1.5975 using the single point stage, has been placed into the solvent vapour annealing chamber and swelled using the swelling protocol outlined in section 3.9.1. The ambient refractive index has been bounded to the interval [1, 1.3] with a step size 0.1 and the thin film refractive index bounded to the interval [1.1, 2] with a step size 0.1. The thin film thickness has been bounded to the interval [250 nm, 600 nm] with step size 1 and the silicon oxide thickness set to 2 nm. Figure 4.12 shows the values found using the fitting protocol outlined in section 3.7. The vertical dotted lines have been added to represent times where the swelling protocol has increased and decreased the nitrogen gas flow and toluene vapour. Horizontal lines have been added to the thickness plot to help the reader. The mean square error is shown in figure 4.13 and the solvent concentration in figure 4.14 using equation 3.15. The thickness of the polystyrene shows a slow uptake of the toluene vapour during the first 4000 seconds. The thickness increases from 275 nm to 300 nm. During this time the polystyrene refractive index increases from [1.6] to [2.0]. The polystyrene refractive index jump from 1.6 to 1.7 passed the 1000 seconds mark and the jump from 1.8 to 2 around the 3000 second mark coincide with jumps in the ambient refractive index. The refractive index of the ambient increases slowly over the course of the first 4000 seconds, which coincides with the increased flow of nitrogen through the toluene. There are areas in the figures where there is noise. The noise manifests itself through back and forth jumps in the refractive index values and jumps in the thickness values. The fitting has trouble around the 450 nm and 500 nm interval, i believe this is the cause of the noise. This is also reflected in the mean square error figure 4.13. The increase of the mean square error at 1500 mark coincides with the noise in the refractive index of the ambient and thin film, and thickness, figure 4.12. The increase of the square error at 2500 and 3000 mark shows sudden drops in the thickness values which also coincide with increase of the refractive index of the thin film. During the maximum swelling interval the mean square error increases from 0.1 to 1. The reflectance during this time decreases creating a gap between the fresnel equations and reflectance measurement, increasing the mean square error. When the slow drying commences at the 5500 second mark, the thickness and mean square

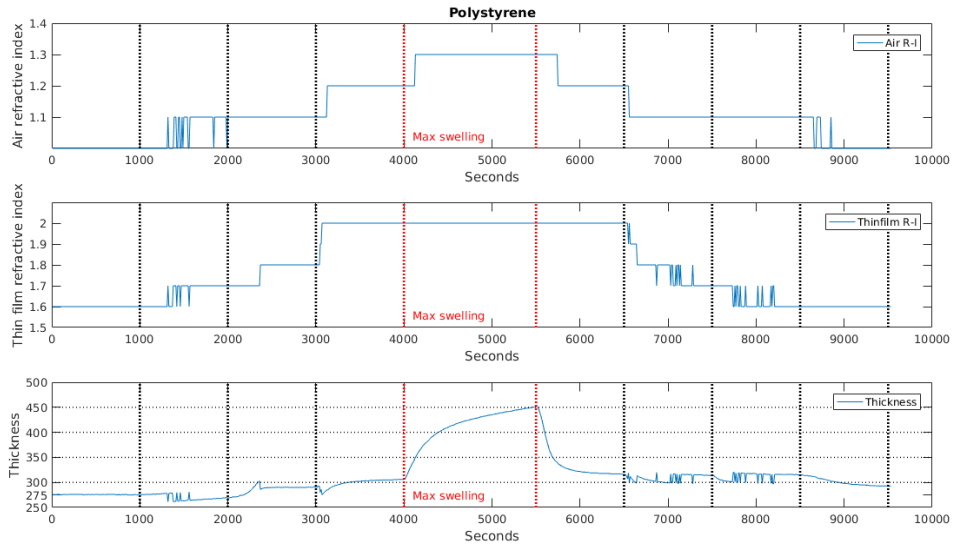


Figure 4.12: The values for the refractive index for the ambient and thin film, and the thickness has been plotted as a function of time for polystyrene. The values have been found using the fitting protocol outlined in 3.7. Vertical dotted lines have been added to represent times where the swelling protocol has increased and decreased the nitrogen gas flow and toluene vapour. The region between the red vertical dotted lines denote the maximum flow through the toluene.

error values drops significantly. The swelling from 300 nm to 450 nm takes roughly 1500 seconds and deswelling to roughly the same thickness takes 500 seconds. The increase in the mean square error after the 6500 second mark is due to the noise in the thin film refractive index.

## 4.5 Polyisoprene

Polyisoprene with a measured thickness of 301 nm and a refractive index 1.4594 using the single point stage, has been placed into the solvent vapour annealing chamber and swelled using the solvent vapour annealing protocol outlined in section 3.9.1. The ambient refractive index has been bounded to the interval  $[1, 1.3]$  with a step size 0.1 and the thin film refractive index bounded to the interval  $[1.4, 2]$  with a step size 0.1. The thin film thickness has been bounded to the interval  $[250 \text{ nm}, 550 \text{ nm}]$  with a step size 1 and the silicon oxide thickness set to 2 nm. Figure 4.16 shows the values found using the fitting protocol outlined in section 3.7. The vertical dotted lines has been added to represent times where the swelling protocol has increased and decreased the nitrogen gas flow and toluene vapour. Horizontal

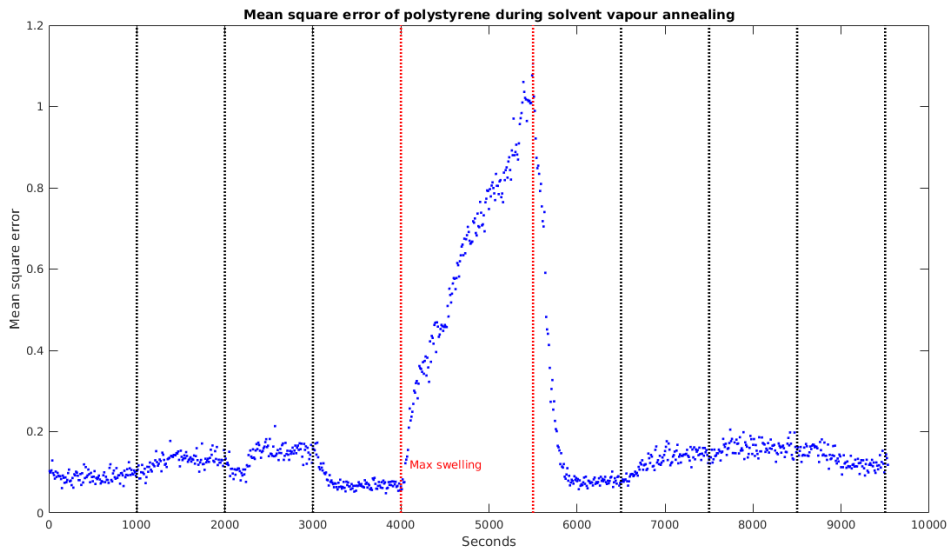


Figure 4.13: The mean square error for the fitting of the fresnel reflectance model on polystyrene reflectance has been plotted as a function of time. The mean square error can be seen to increase at the 1500 and 2500 mark due to the noise in the modelling and drop in thickness values. The mean square error increases from 0.1 to 1 during the max toluene swelling, this is due to the reflectance measurements decreasing in value during this time and creating a gap between the fresnel reflectance equation and reflectance. The increase in the mean square error after the 6500 second mark is due to the noise in the thin film refractive index.

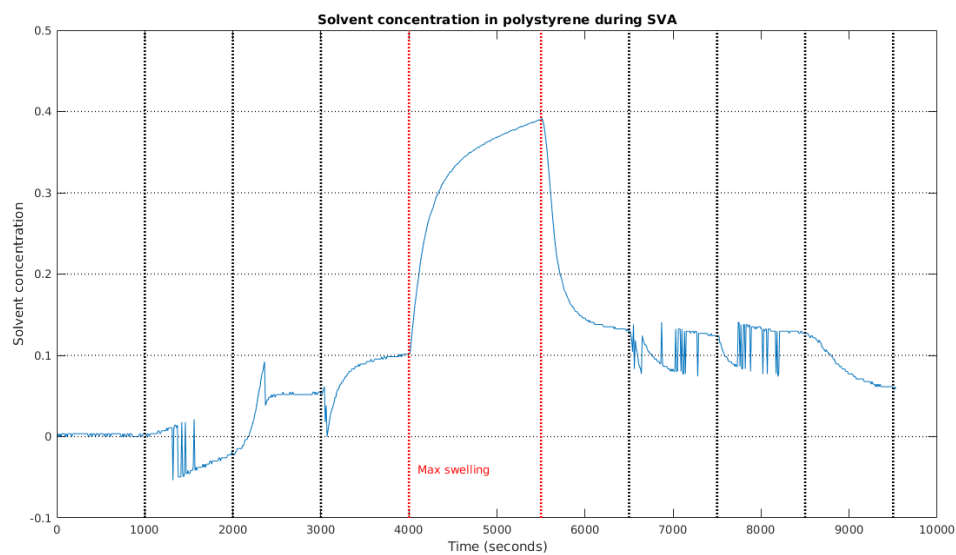


Figure 4.14: The solvent concentration in the polystyrene as a function of time.

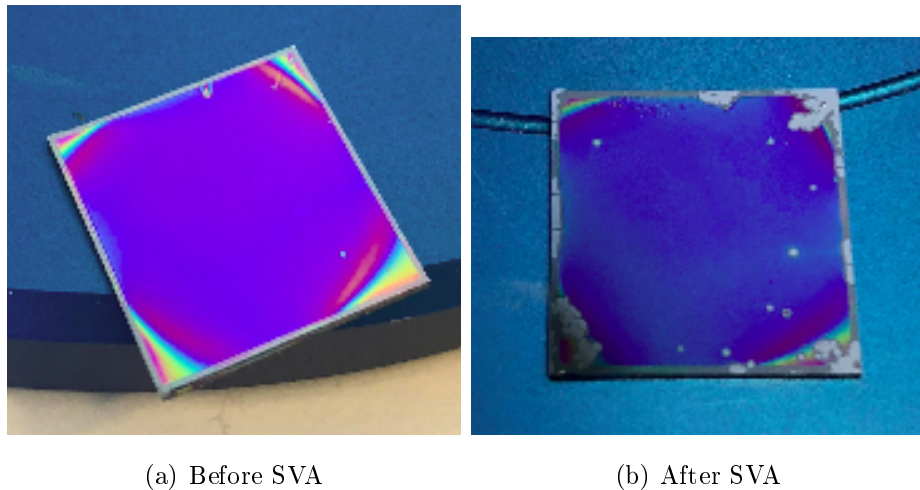


Figure 4.15: Before and after solvent vapour annealing photos of polystyrene

lines have been added to the thickness plot to help the reader. The thickness of the polyisoprene shows a slow uptake of the toluene vapour during the first 4000 seconds. The thickness of polyisoprene increases from 300 nm to 400 nm. During this time the polyisoprene refractive index increases from [1.4] to [1.6]. The jumps in the polyisoprene refractive index at the 2000 and 3000 mark coincide with little spikes in the thickness values. The ambient refractive index at the 3000 second mark is erratic, and further along around the 3500 second mark the ambient refractive index drops back to 1. During the maximum swelling of the polyisoprene, the refractive indices and thickness increase. There are dips in the thickness during the maximum swelling which coincide with the increase of the polyisoprene refractive index, 1.6 to 1.7 and 1.7 to 1.8, and increase of the ambient refractive index, 1.2 to 1.3. Deswelling starts at the 5500 second mark and the thickness drops from 550 nm to 400 nm with in 1000 seconds. The thickness measurements continue to decrease and the drops in thickness coincide with the decrease in polyisoprene refractive index. The mean square error increases around the 2000 second mark when the ambient refractive index and the polyisoprene refractive index increase. The mean square error increases during the maximum swelling interval from 0.1 to 0.8. During the maximum swelling there are three mini spikes in the mean square error, the first increase coincides with the increase of the ambient refractive index from 1.1 to 1.2. The second coincides with the increase of both the ambient and polyisoprene refractive index, from 1.2 to 1.3 and 1.6 to 1.7 respectively. The third coincides with the increase of the polyisoprene refractive index from 1.7 to 1.8. The mean square error variation after the maximum swelling coincide with the decreases polyisoprene refractive index. The solvent concentration in the thin film as a function of time is shown in figure 4.18.

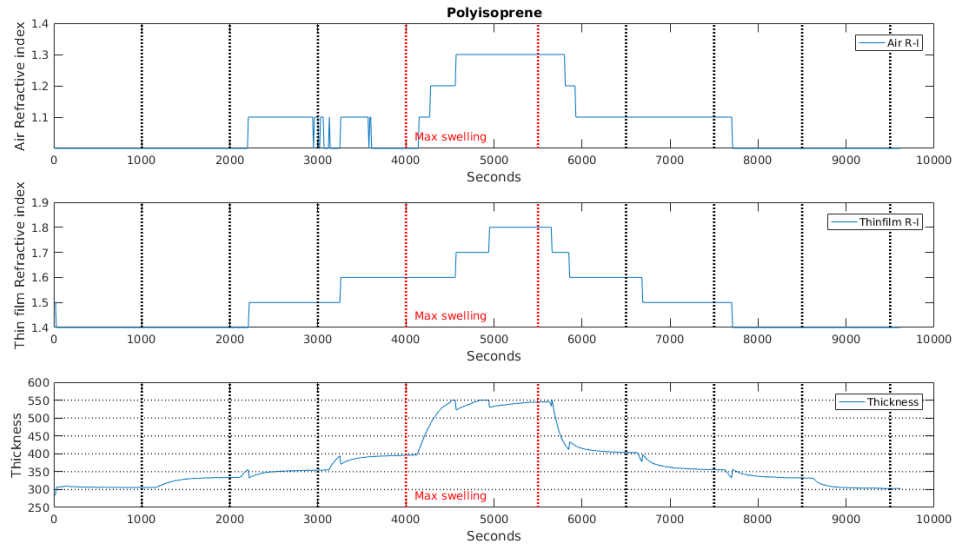


Figure 4.16: The values for the refractive index for the ambient and thin film, and the thickness has been plotted as a function of time for polyisoprene. The values have been found using the fitting protocol outlined in 3.7. Vertical dotted lines have been added to represent times where the swelling protocol has increased and decreased the nitrogen gas flow and toluene vapour. The region between the red vertical dotted lines denote the maximum flow through the toluene.

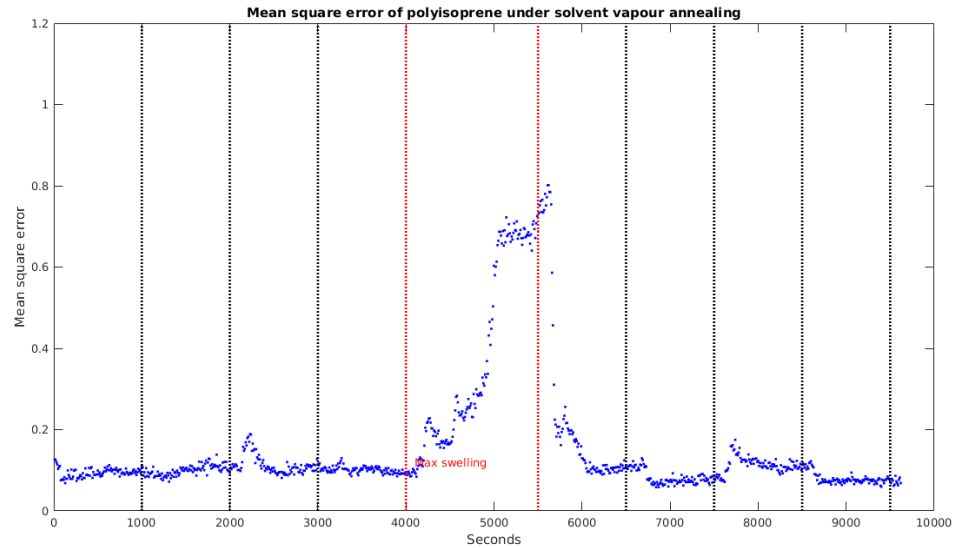


Figure 4.17: The mean square error for the fitting of the fresnel reflectance model on polyisoprene reflectance has been plotted as a function of time.

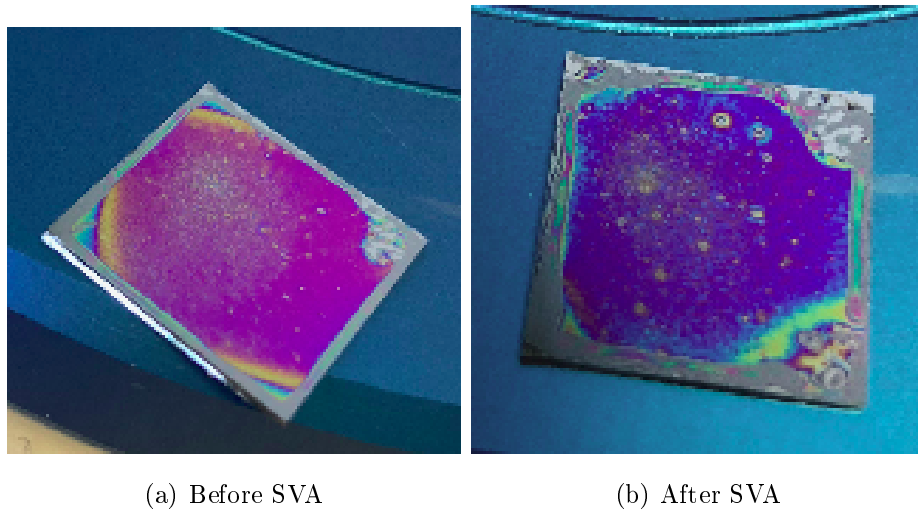


Figure 4.19: Before and after solvent vapour annealing photos of polyisoprene

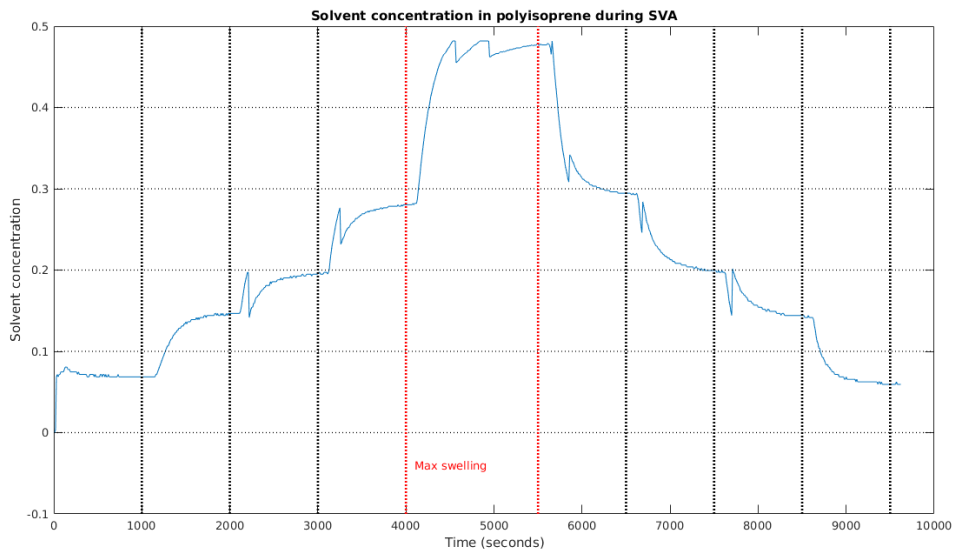


Figure 4.18: The solvent concentration in the polyisoprene plotted as a function of time.

## 4.6 Polystyrene-*b*-polyisoprene

Polystyrene-*b*-polyisoprene with a measured thickness of 97.3 nm and a refractive index 1.5659, using the single point stage, has been placed into the solvent vapour annealing chamber and swelled using the solvent vapour annealing protocol outlined in section 3.9.1. The ambient refractive index has been bounded to the interval [1, 1.3] with a step size 0.1 and the thin film refractive index bounded to the interval [1.5, 2] with a step size 0.1. The thin film thickness has been bounded to the interval

[95 nm, 200 nm] with a step size 1 and the silicon oxide thickness set to 2 nm. Figure 4.20 shows the values found using the fitting protocol outlined in section 3.7. The vertical dotted lines has been added to represent times where the swelling protocol has increased and decreased the nitrogen gas flow and toluene vapour. Horizontal lines have been added to the thickness plot to help the reader. From the ambient refractive index figure it can be seen that the fitting sets the refractive index to 1.2 for roughly the first 1500 seconds then decreases the index to 1.1. The refractive index of 1.1 is held for roughly 1500 seconds then decreases to 1 and held until the interval of maximum toluene swelling. The refractive index of the polymer is fitted to 1.5 for roughly the first 4000 seconds. During the first 4000 seconds, the thickness increases from 106 nm to 141 nm. Three things should be highlighted from this model fitting in the first 4000 seconds. The first is that the ambient refractive index begins at 1.2 and drops when slowly increasing toluene vapour. The second is that the refractive index of the polymer is constant until maximum toluene swelling. The third is that the thickness values increase during the slow swelling while the ambient refractive index drops and the refractive index for the polymer does not increase. During the maximum swelling of the polystyrene-*b*-polyisoprene, the refractive indices and thickness increase. The refractive index for the ambient increases to 1.1 for the maximum swelling interval and the refractive index for the polymer increases from 1.5 to 2 in time span of roughly 1500 seconds. The thickness increase also in this time. The noise in the refractive index coincides with the noise in the thickness values. The refractive index for the ambient drops back to 1 at the 5500 mark and increases as the toluene vapour decreases. The refractive index for the polymer quickly drops down to 1.5 when drying commences. The thickness values also decrease when drying. The mean square error can be seen in figure 4.21. The mean square error values are oddly small during the solvent vapour annealing process. The general tendencies is that the mean square error decreases during the first 4000 seconds. There is a spike around the 4500 second mark which does not coincide with anything seen in figure 4.20. After the interval with maximum toluene swelling the mean square error values increase. The solvent concentration in the polystyrene-*b*-polyisoprene as a function of time is shown in figure 4.22.

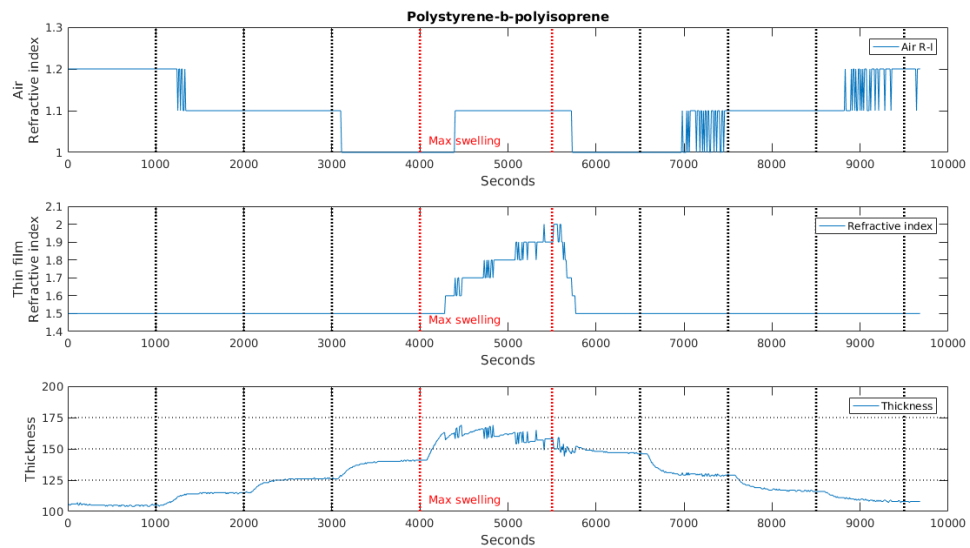


Figure 4.20: The values for the refractive index for the ambient and thin film, and the thickness has been plotted as a function of time for polystyrene-*b*-polyisoprene. The values have been found using the fitting protocol outlined in 3.7. Vertical dotted lines have been added to represent times where the swelling protocol has increased and decreased the nitrogen gas flow and toluene vapour. The area between the red vertical dotted lines denote the maximum flow through the toluene.

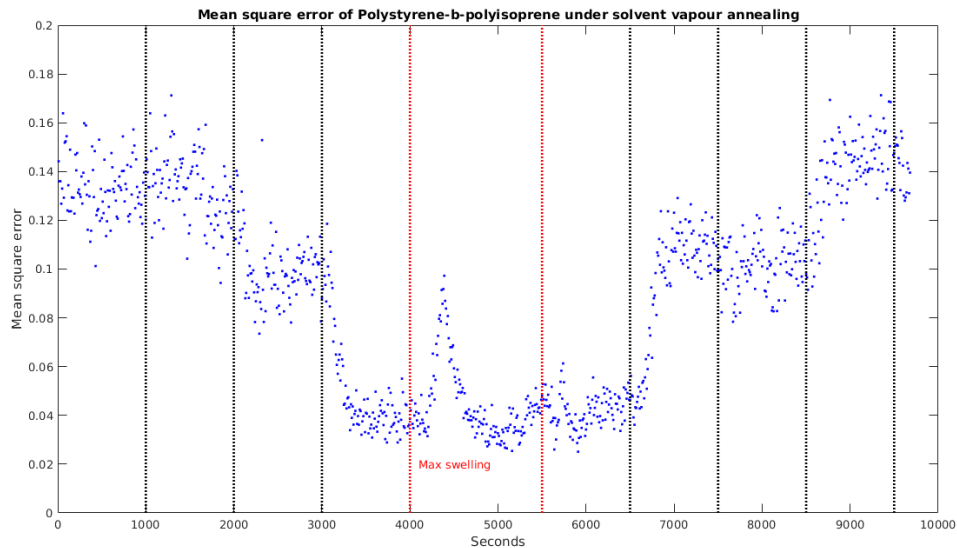


Figure 4.21: The mean square error for the fitting of the fresnel reflectance model on polystyrene-b-polyisoprene reflectance has been plotted as a function of time. The mean square error decreases during the first 4000 seconds. There is a spike around the 4500 second mark which does not coincide with anything seen in figure 4.20. It then increases during drying.

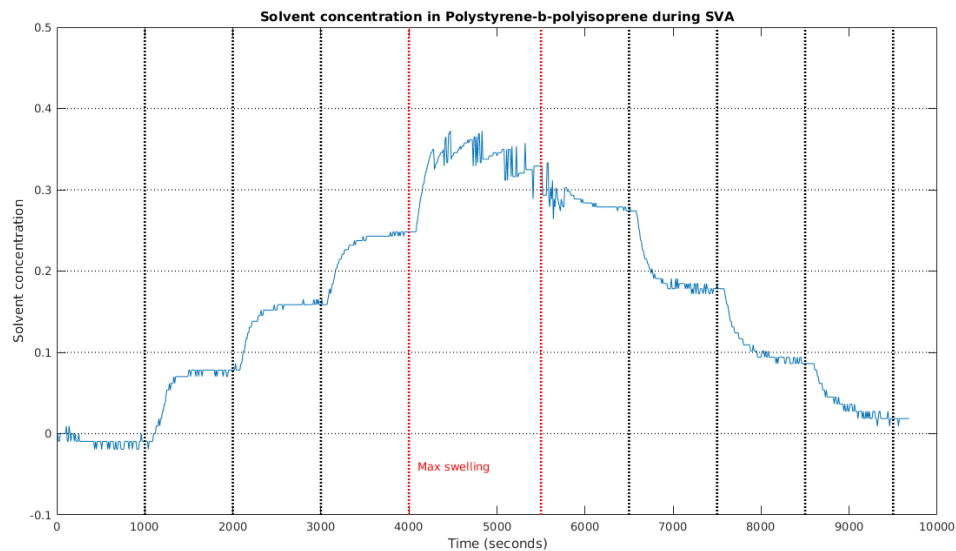


Figure 4.22: The solvent concentration in the polystyrene-b-polyisoprene plotted as a function of time.

## 4.7 Measurement table and model atble

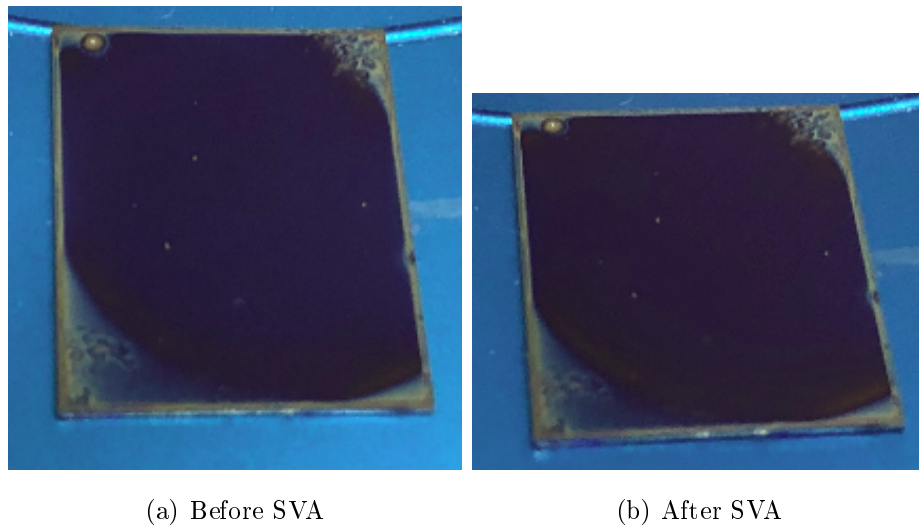


Figure 4.23: Before and after solvent vapour annealing photos of polystyrene-b-polyisoprene

Table 4.2:

| Experiment  | Polystyrene | Polyisoprene | Polystyrene-b-polyisoprene |
|---|-------------|--------------|----------------------------|
| Single Point Stage<br>SVA fitting<br>Ellipsometry |             |              |                            |
| X-ray Reflectometry                               |             |              |                            |

Table 4.3:

| SVA          | Ambient Refractive index, step size = 0.1 | Thin film Refractive index, step size = 0.1 | Thin film thickness, step size = 1 |
|--------------|---|---|------------------------------------|
| Polystyrene  | 1 – 1.3                                   | 1.1 – 2                                     | 250 – 600                          |
| Polyisoprene | 1 – 1.3                                   | 1.4 – 2                                     | 250 – 550                          |
| PS-b-PI      | 1 – 1.3                                   | 1.5 – 2                                     | 95 – 200                           |

# Chapter 5

## Discussion

### 5.1 Experimental setup

The experimental setup can be used in two ways. The first way with the optical fiber in the single point stage and the second way with the optical fiber in the solvent vapour annealing chamber. When the optical fiber is fitted into the solvent vapour annealing chamber, the light must pass through a sapphire lens. This causes a great deal of reflected light and affects the reflectance measurements taken. This can be seen by holding the static measurements seen in table 3.2 against the first fitted thickness values found in the figures for each polymer in chapter 4. The effects may be small at the beginning of the solvent vapour annealing when the polymer has not swelled, but during swelling the reflectance measurements drop and can be zero in some intervals. The sapphire lens effectively increases the dark measurement and when calculating the reflectance, since the dark measurement is in the denominator, lowers the reflectance measurements. It can be seen when plotting the reflectance measurements alone with no strict axis interval that some of the reflectance measurements drop below zero, as seen in figure 5.1. The reason for this is unknown. Reflectance measurements close to zero can be seen in figure 5.2. The dark measurements are taken when the optical fiber is fitted into the solvent vapour annealing chamber with a piece of black fabric where the wafer would lay. The black fabric is a piece of black cotton. The effect, if there is any, of the black fabric has not been investigated. The distance from the wafer to the optical fiber is important, as it is seen to shift the whole reflectance measurement up and down the y axis. Up if the distance increases and down if it decreases. It is therefore very important to use a step wafer where the thickness are known to adjust the single point stage before a static measurement of a wafer with a thin film. When the optical fiber is placed in the solvent vapour annealing chamber the distance between the optical

fiber and the wafer is much greater than it is intended thus the sapphire lens is used to focus the light to illuminate the wafer. Calibrating the solvent vapour annealing setup is impossible since the chamber is not big enough for the step wafer to be place in the chamber. Taking the best reference and dark measurement is key to a good reflectance measurement for the thin film, though it seems that the best measurement is impossible. A measurement close to good can be achieved as seen in the fitting of the fresnel equations using the homopolymers reflectance data.

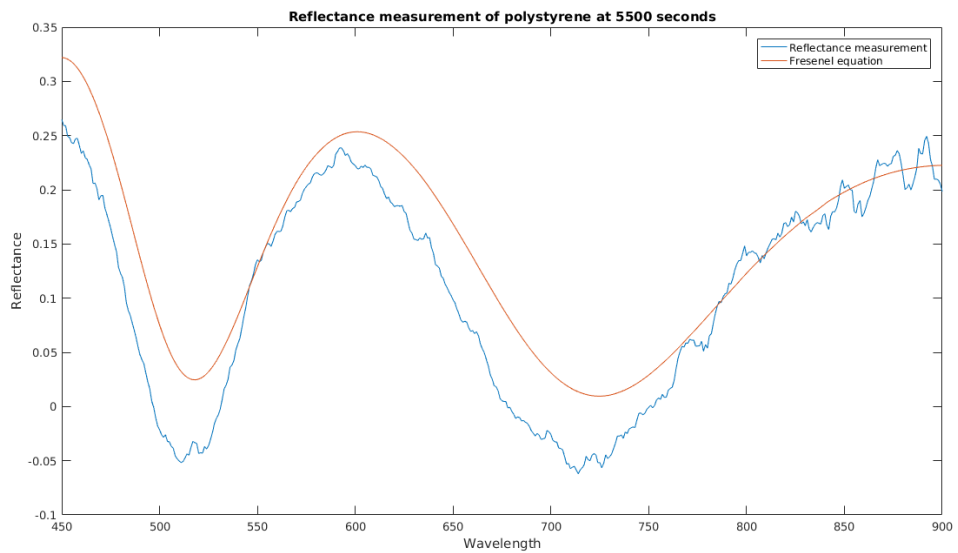


Figure 5.1: The reflectance measurement for polystyrene at time 5500 seconds with the best fitting fresnel equation plotted. It can be seen that the reflectance measurement drops compared to the theoretical model. The cause for the drop in reflectance is unknown. This is the reason for the increased mean square error.

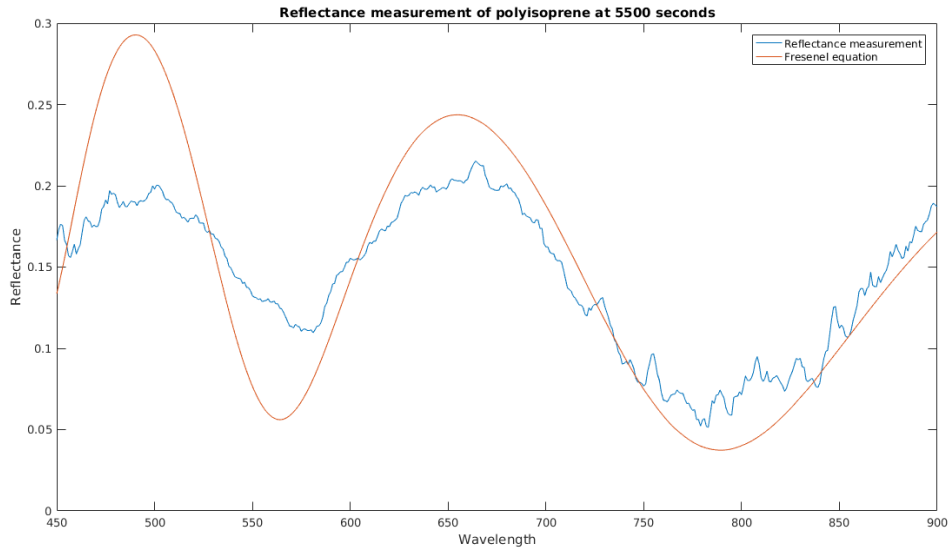


Figure 5.2: The reflectance measurement for polyisoprene at time 5500 seconds with the best fitting fresnel equation plotted. It can be seen that the reflectance measurement drops compared to the theoretical model. The cause for the drop in reflectance is unknown. This is the reason for the increased mean square error.

## 5.2 Refractive index dispersion of polymers and absorption

The refractive index dispersion of the polymers has been shown in figure 4.5 using the values given by the experimental method ellipsometry. It can be seen that the refractive index varies across the wavelengths. Polystyrene's refractive index does not vary as greatly as polyisoprene and polystyrene-b-polyisoprene. The fitting has not taken into account the dispersion of the refractive index, instead the constant refractive index has been used. It is unknown how the uptake of the solvent would effect the dispersion and how the dispersion would effect the reflectance measurements. An analytical study of the fresnel equations would be needed to fully grasp how changing the refractive indices impact the reflectance curves. Absorption is another parameter that can effect the reflectance measurements. Absorption is not present in the fresnel equations and can be the cause for the divergence between the reflectance measurements and the fresnel equations.

### 5.3 Refractive index of toluene vapour

The conclusion of the solvent vapour annealing ambient study was that during the solvent vapour annealing protocol the ambient increases from 1 to 1.3. The ambient starts off as air with a refractive index of 1 and as the toluene vapour starts to fill the chamber, the air and the toluene vapour mix. The refractive index of 1.3 seems reasonable for the toluene vapour. My argument for this is that vapour is in a gas state below its critical temperature but can liquefy due to increase in pressure. The refractive index for toluene in a liquid state is 1.496 [15]. The refractive index of toluene vapour can not be greater than the refractive index for toluene in a liquid state, so the vapour refractive index must be bounded by an interval spanning 1 to 1.496. When swelling there is a possibility that condensation forms in the chamber, this has not been investigated.

### 5.4 Mean square error fitting

The mean square error fitting has been used as it was the fitting protocol used in the nano-calc software and other fitting methods have not been studied or implemented. The interval of fitting has been chosen to run from 450 nm to 900 nm. This interval has been the easiest to fit to due to the reflectance measurements being smooth in this region and features present in this interval to fit to. The fitting of the reflectance measurements follow the features seen in the fresnel equation but when swelling commences the reflectance measurements shift and drop. This can be seen in the figures 5.1 and 5.2. Both figures have been taken at the 5500 second mark, at the end of the max swelling interval and the reflectance measurements have shifted and dropped with respect to the theoretical model. The way the fitting has been implemented into matlab can also be critiqued. The fitting loads a reflectance measurements and loops through the refractive indices for air and the thin film and the thickness values. For polystyrene this amounted to 13,380,120 combinations taking roughly 75 minutes to loop through, for polyisoprene 8,116,164 combinations taking roughly 44 minutes and polystyrene-b-polyisoprene 2,462,592 combinations roughly 13 minutes. The fitting on the two homopolymers shown results that are in tune with what is expected. As the nitrogen flows through the toluene solvent, the toluene vapour increases in the chamber and the refractive index for the ambient increases. This can be also seen for the thin films refractive index as we expect solvent uptake. The thickness values increases as well marking the point when the solvent vapour annealing protocol has increased and decreased the channels.

The ambient refractive index is normally set to 1 when making static measurements. During the ambient study the reflectance measurements shows a decrease during swelling. The fitting increases the refractive index for the ambient and the fresnel equations follow the reflectance measurements well. The increases in the mean square error values for the ambient study can be caused by the large step sizes in the refractive index. The step size used in the fitting have been set crudely. The step size for the thickness is set to 1. Since we are working on the nanoscale, having thickness values with decimals does not shine light on anything interesting when looking at the thickness measurements. The step size for both refractive indices has been set to 0.1. This has been set to one decimal for two reasons. The first reason is that more values the fitting has to loop through, the long the fitting will take, and the second reason is that a finer step size would not contribute useful information to the thickness fitting, what is important is that there is an increase.

## 5.5 Solvent vapour annealing

In the solvent vapour annealing protocol the nitrogen flow has been set to be constant through out the protocol. The assumption is that holding the flow constant will hold the vapour pressure in the chamber constant. This is a crude assumption since the variables flow and pressure are heavily dependant on the tube sizing, the volume of the solvent vapour annealing chamber, the volume of the bubbler and the volume of liquid present in the bubbler. Taking these variable into account and calculating the vapour pressure constitutes a research project in itself. The solvent vapour annealing protocol has been programmed into a script which the mass flow controllers software could read and run. As seen in figure 3.7, the increases and decreases of flow controlled by the mass flow controllers happen before they should. Each step apart from the maximum swelling should have a length of 1000 seconds. The solvent vapour annealing time file was not saved, so i can not precisely determine when the mass flow controllers changed the flow but the solvent vapour annealing protocol was close to what was scripted.

## 5.6 Polystyrene and Polyisoprene

When fitting the fresnel equations using the reflectance measurements, the homopolymer results behaved as anticipated but the diblock copolymer results were the opposite to what was expected. The expected results were an increase in ambient refractive index and thin film refractive index which coincided with the increase of

toluene vapour present in the chamber. What i expected with the thickness results was an increase in thickness starting every time there was an increase of toluene vapour. These expectations of how the results should look were seen. The thickness results show a 'shark dorsal fin' during the maximum swelling region. One can think that if the maximum swelling was left the thickness would reach a constant value. There is an interval of time between a change from the mass flow controllers to the beginning of a change in the polymers, this is called a response time. [ADD Values]. The mean square error for both the polystyrene and polyisoprene show a constant mean square error expect for when the maximum swelling commences. This is because the fit and the reflectance data do not matching up. In figure 5.1 it can be seen that the fit for polystyrene is higher than the polystyrene reflectance measurement. In figure 5.2 the amplitude of the polyisoprene fit is much greater than the polyisoprene reflectance measurement. During the swelling it is apparent that something is happening that the fresnel equations do not accommodate for. This could be a multitude of things since the fresnel equations are simple. The fresnel equations do not account for an inhomogeneous increase in thickness. The fresnel equations assume a homogenous increase throughout the thin film but since there are thermodynamic forces, interaction forces between the monomers and the spread of vapour in the chamber, the thin film will increase in an inhomogeneous way. The roughness, variation of thickness in the thin film, can play a role as this can cause diffusive reflection and decrease the reflectance measurements. The polystyrene thickness values are erratic in the swelling and the deswelling but steady in the maximum swelling region. The same can be said for polyisoprene's swelling and deswelling, but in the maximum swelling region the polyisoprene thickness drop twice and returns to the maximum thickness again of 550 nm. Each drop is roughly 25 nm. The drops in thickness could be the polyisoprene rearranging and the sharp drop look steep because the measurement timescale and the timescale of the polymer do not match. Measurements are taken every 10 seconds, thus the thickness values can be thought of as discrete.

## 5.7 Polystyrene-b-polyisoprene

The fitting for the diblock copolymer polystyrene-b-polyisoprene behaves strangely. The fitting shows an ambient refractive index starting at 1.2 and decreasing in value as the toluene vapour increases. The thin film refractive index does not increase until the solvent vapour annealing protocol reaches the region of maximum swelling. In this region the thin film refractive index climbs rapidly and is erratic throughout

the maximum swelling. The thickness does increase nicely through out the solvent vapour annealing protocol. The mean square error is large at the start of the swelling and decreases during the swelling. The mean square error does peak during the swelling, this coincides with the fitting protocol changing the ambient refractive index from 1 to 1.1. The fitting implemented has used one layer with a varying real refractive index. This simple model does not capture the actual structure seen with diblock copolymers. Diblock copolymers organises itself into a multilayer system consisting of a layer consisting of the A block and the next layer consisting of the B block, an A-B-A-B thin film structure, which can consist of many layers. This structure is not seen in the homopolymers as they consist of one monomer repeated. Fitting for this multilayer thin film with my fitting protocol requires a large amount of computer power. When adding a new variable into the protocol, you are effectively multiplying the amount of values the new variable has onto the amount of combination the fitting protocol, increasing the total amount of calculations the fitting protocol has to calculate. The fitting protocol is not suited to diblock copolymers.

# Chapter 6

## Conclusion

In the course of this thesis using the optical spectral reflectance experimental technique, the goals have been to investigate the advantages and limitations of the experimental technique when determining the thickness of thin polymer films during solvent vapour annealing, investigation of optimal modelling and fitting method to determine thickness of homopolymers during solvent vapour annealing and an investigation into whether the same thickness determination could be used to determine thickness of a thin film such as the diblock copolymer polystyrene-*b*-polyisoprene. The advantages of this experimental technique is that the modelling aspect uses the fresnel equations and are easily calculated. These are easy to understand and easy to model multiply layers since the fresnel equations are recursive. The limitations of this technique is that the dark measurements can greatly impact the reflectance measurements of a thin films. Care is need when performing a dark measurement and a proper technique is need for the solvent vapour annealing chamber as there is light reflected back through the optical fiber due to a focusing lens. The modelling of the homopolymers polystyrene and polyisoprene has used the fresnel equation shown in equation 2.49. This model assumes that the homopolymers consist of one layer and has a homogeneous thickness and real refractive index. The fitting implemented is a script finding the lowest mean square error for each reflectance measurement. From the result it can be seen that the thickness determination can be found during the solvent vapour annealing when modelling the layer as a homogeneous thickness with real refractive indices. Using the same model to determine the thickness of the diblock copolymer polystyrene-*b*-polyisoprene shows strange results that does not reflect the solvent vapour annealing process. The modelling and fitting done in this thesis seems optimal for homopolymers lacking structure but fails when applied to polymer systems with structure.

# Chapter 7

## Bibliography

- [1] Jianqi Zhang, Dorthe Posselt, Detlef-M. Smilgies, Jan Perlich, Konstantinos Kyriakos, Sebastian Jaksch, and Christine M. Papadakis. Lamellar diblock copolymer thin films during solvent vapor annealing studied by gisaxs: Different behavior of parallel and perpendicular lamellae. *Macromolecules*, 47(16):5711–5718, 2014. PMID: 25197146.
- [2] H. Fujiwara. *Spectroscopic Ellipsometry: Principles and Applications*. Wiley, 2007.
- [3] H.G. Tompkins and J.N. Hilfiker. *Spectroscopic Ellipsometry: Practical Application to Thin Film Characterization*. Materials Characterization and Analysis Collection. Momentum Press, 2015.
- [4] H.C. Ohanian and J.T. Markert. *Physics for Engineers and Scientists*. Motion, force, and energy oscillations, waves, and fluids temperature, heat, and thermodynamics. W. W. Norton & Company, 2007.
- [5] G.R. Strobl. *The Physics of Polymers: Concepts for Understanding Their Structures and Behavior*. Springer Berlin Heidelberg, 2007.
- [6] Frank S. Bates and Glenn Fredrickson. Block copolymer thermodynamics: Theory and experiment. *Annual review of physical chemistry*, 41:525–57, 10 1990.
- [7] Daniel J. Kozuch, Wenlin Zhang, and Scott T. Milner. Predicting the flory-huggins parameter for polymers with stiffness mismatch from molecular dynamics simulations. *Polymers*, 8(6), 2016.
- [8] M.C. Petty. *Molecular Electronics: From Principles to Practice*. Wiley Series in Materials for Electronic & Optoelectronic Applications. Wiley, 2008.

- [9] Frank S. Bates and Glenn Fredrickson. Block copolymers - designer soft materials. *Physics Today*, 52(2):32, 1999.
- [10] Christophe Sinturel, Marylène Vayer, Michael Morris, and Marc A. Hillmyer. Solvent vapor annealing of block polymer thin films. *Macromolecules*, 46(14):5399–5415, 2013.
- [11] Dorthe Posselt, Jianqi Zhang, Detlef-M. Smilgies, Anatoly V. Berezkin, Igor I. Potemkin, and Christine M. Papadakis. Restructuring in block copolymer thin films: In situ gisaxs investigations during solvent vapor annealing. *Progress in Polymer Science*, 66:80–115, 2017.
- [12] Ocean Optics. *NanoCalc Software Manual*, version 4 edition, 2014.
- [13] Bronkhorst. *El-Flow® select Brochure*. Available at <https://www.bronkhorst.com/products/gas-flow/el-flow-select/f-201cv/>.
- [14] A. Baruth, Myungeun Seo, Chun Hao Lin, Kern Walster, Arjun Shankar, Marc A. Hillmyer, and C. Leighton. Optimization of long-range order in solvent vapor annealed poly(styrene)-block-poly(lactide) thin films for nanolithography. *ACS Applied Materials & Interfaces*, 6(16):13770–13781, 2014. PMID: 25029410.
- [15] Sigma-aldrich toluene data sheet. <https://www.sigmaaldrich.com/chemistry/solvents/toluene-center.html>. Accessed: 26-03-2019.

# Appendix A

## Fresnel functions and Dispersion files

### A.1 Functions

```
1 function [r_jk] = fresnel_am_s(n_j,n_k)
2
3 r_jk = (n_k-n_j)./(n_k+n_j);
4
5 end
```

```
1 function [beta] = filmphasethickness(lamda,n_k,d_k)
2
3 beta = (2.*pi.*d_k.*n_k)./(lamda);
4
5 end
```

```
1 function [r_jkl] = fresnel_am_tf_s(n_j,n_k,n_l,d_k, lamda)
2
3 r_jkl = (fresnel_am_s(n_j,n_k)+fresnel_am_s(n_k,n_l) ...
4 .*exp(-2i.*filmphasethickness(lamda,n_k,d_k)))./ ...
5 (1+fresnel_am_s(n_j,n_k).*fresnel_am_s(n_k,n_l) ...
6 .*exp(-2.*1i.*filmphasethickness(lamda,n_k,d_k)));
7
8 end
```

```
1 function [r_jklm] = fresnel_am_tf_lay_sub(n_j,n_k,n_l,n_m,d_k,d_l, lamda)
2
3 r_jklm = (fresnel_am_s(n_j,n_k)+ fresnel_am_tf_s(n_k,n_l,n_m,d_l, lamda).* ...
4 exp(-2i.*filmphasethickness(lamda,n_k,d_k))) ...
5 ./ (1+fresnel_am_s(n_j,n_k).*fresnel_am_tf_s(n_k,n_l,n_m,d_l, lamda).* ...
6 exp(-2i.*filmphasethickness(lamda,n_k,d_k)));
7
8 end
```

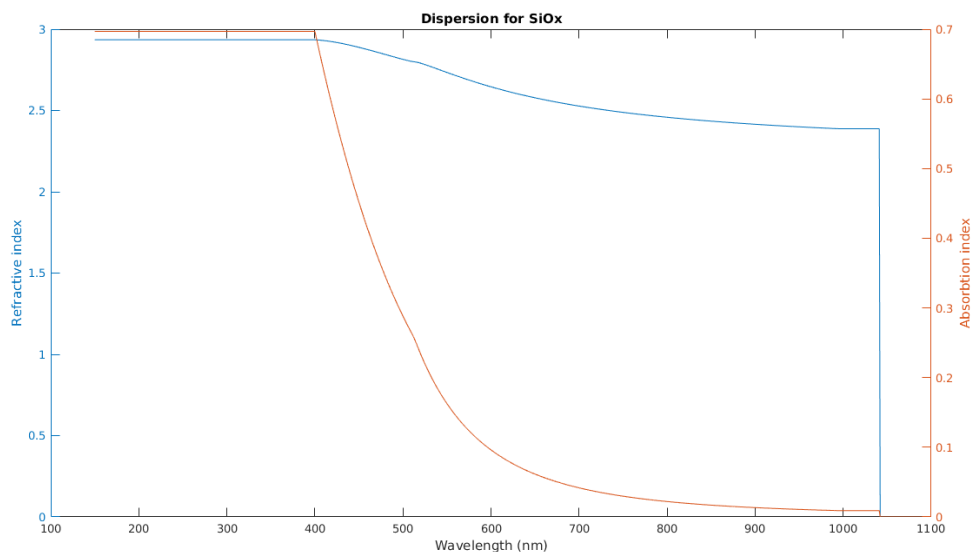
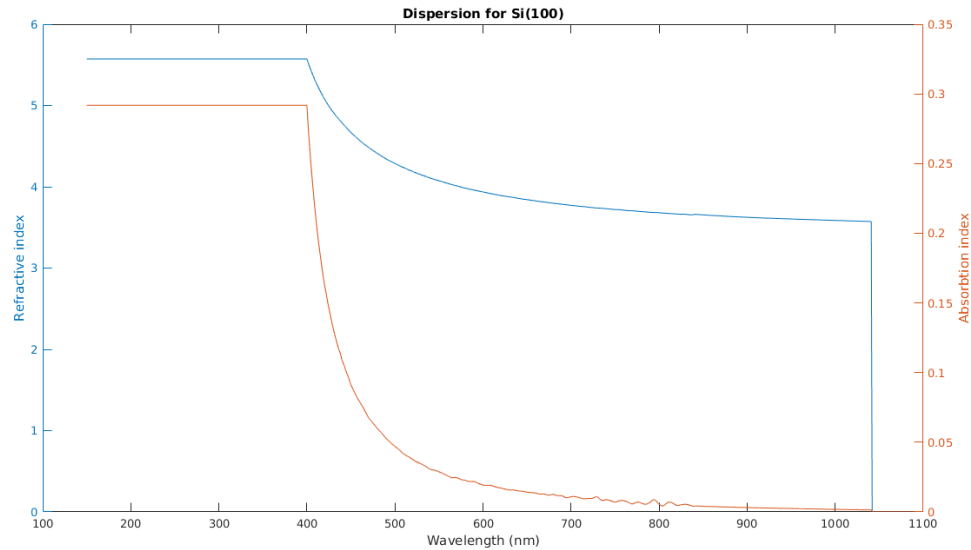
```
1 function n_c = cauchy(lamda,A,B,C)
2
```

```

3 n_c = A + (B./(lambda.^2)) + (C./(lambda.^4));
4
5 end

```

## A.2 Dispersion files curves



```

1 clear all
2 close all
3
4 %% Dispersion %
5 % Dispersion %
6 %% Dispersion %

```

```
7
8 load dispersion_Si(100).dat
9 wl = dispersion_Si_100(:,1);
10 x = dispersion_Si_100(:,2);
11 y = dispersion_Si_100(:,3);
12
13 load dispersion_SiOx.dat
14 wl2 = dispersion_SiOx(:,1);
15 x2 = dispersion_SiOx(:,2);
16 y2 = dispersion_SiOx(:,3);
17
18 %%%%%%%%%%%%%%
19 % Plotting %
20 %%%%%%%%%%%%%%
21
22 figure
23 yyaxis left
24 plot(wl,x)
25 title('Dispersion for Si(100)')
26 xlabel('Wavelength (nm)')
27 ylabel('Refractive index')
28 xlim([100 1100])
29
30 yyaxis right
31 plot(wl,y)
32 ylabel('Absorbtion index')
33
34
35 figure
36 yyaxis left
37 plot(wl2,x2)
38 title('Dispersion for SiOx')
39 xlabel('Wavelength (nm)')
40 ylabel('Refractive index')
41 xlim([100 1100])
42
43 yyaxis right
44 plot(wl2,y2)
45 ylabel('Absorbtion index')
```

# Appendix B

## Scripts

### B.1 SVA Protocol - slowslow.fps

```
1 [Generator]
2 Application=FlowPlot
3 Version=V3.34
4 [Script]
5 Repeat=1
6 SendSetpointAfter=false
7 001="1.0;    0.0;  2;  9"
8 002="1.0;    0.0;  3;  9"
9 003="1.0;    0.0;  1;  9"
10 004="1000.0;   50.0;  1;  9"
11 005="1.0;    37.5;  1;  9"
12 006="1000.0;   25.0;  2;  9"
13 007="1.0;    25.0;  1;  9"
14 008="1000.0;   50.0;  2;  9"
15 009="1.0;    12.5;  1;  9"
16 010="1000.0;   75.0;  2;  9"
17 011="1.0;    0.0;  1;  9"
18 012="1500.0;   100.0; 2;  9"
19 013="1.0;    12.5;  1;  9"
20 014="1000.0;   75.0;  2;  9"
21 015="1.0;    25.0;  1;  9"
22 016="1000.0;   50.0;  2;  9"
23 017="1.0;    37.5;  1;  9"
24 018="1000.0;   25.0;  2;  9"
25 019="1.0;    50.0;  1;  9"
26 020="1000.0;   0.0;  2;  9"
```

### B.2 Light Source fluctuation study

```
1 clear all
2 close all
```

```

3
4 %%%%%%
5 % Load data %
6 %%%%%%
7
8 load daystudyreflectance
9 y = transpose(daystudyreflectance);
10 arraylength = length(daystudyreflectance(:,1)) ;
11
12 %%%%%%
13 % Physics %
14 %%%%%%
15
16 wavelength = [400:1041];
17
18 %%%%%%
19 % Plotting %
20 %%%%%%
21
22 hold on
23
24 for q = 1: arraylength
25
26
27 plot(wavelength,y(:,q))
28 title('Light Source fluctuation study at different times of the day')
29 xlabel('Wavelength (nm)')
30 ylabel('Reflectance')
31 legend('10.47','11.19','11.49','12.19','12.49',
32 '13.19','13.49','14.19','14.49','15.19','15.49','16.19','16.49','17.19')
33 axis([400 1041 0 1])
34
35 end
36
37 hold off

```

### B.3 Nano-Calc simulated reflectance curve

```

1 clear all
2 close all
3
4
5 %%%%%%
6 % Air_SI(100)_Air.xy %
7 %%%%%%
8
9 %%%%%%
10 % Load data %
11 %%%%%%
12
13 load Air_SI(100)_Air.xy

```

```

14
15 x = Air_SI_100__Air(:,1);
16 y = Air_SI_100__Air(:,2);
17
18
19 %%%%%%
20 % Physics %
21 %%%%%%
22
23 wavelength = [400:1041];
24
25 %%%%%%
26 % Refractive index %
27 %%%%%%
28
29 n_0 = 1;
30
31 load dispersion_Si(100).dat
32 disp = dispersion_Si_100_(251:1:892,:);
33 n_1 = transpose(disp(:,2))-li.*transpose(disp(:,3));
34
35
36
37 %%%%%%
38 % Calculations %
39 %%%%%%
40
41 r_01 = fresnel_am_s(n_0,n_1)
42
43 R_01 = r_01.*conj(r_01);
44
45 plot(x,y,'g',wavelength,R_01,'--k')
46 title([{'Fresnel reflectance equation plotted on NanoCalc simulated reflectance ...' 'curve'}])
47 xlabel('Wavelength(nm)')
48 ylabel('Reflectance(%)')
49 legend('Simulation','Fresnel')

```

```

1 clear all
2 close all
3
4
5 %%%%%%
6 % Air_n1_5_SI(100)_Air.xy %
7 %%%%%%
8
9 %%%%%%
10 % Load data %
11 %%%%%%
12
13 load Air_n1_5_SI(100)_Air.xy
14
15 x = Air_n1_5_SI_100__Air(:,1);

```

```

16 y = Air_n1_5_SI_100_Air(:,2);
17
18
19 %%%%%%
20 % Physics %
21 %%%%%%
22
23 wavelength = [400:1041];
24
25 %%%%%%
26 % Refractive index %
27 %%%%%%
28
29 n_0 = 1;
30 n_1 = 1.5;
31
32 load dispersion_Si(100).dat
33 disp = dispersion_Si_100_(251:1:892,:);
34 n_2 = transpose(disp(:,2))-1i.*transpose(disp(:,3));
35
36 %%%%%%
37 % Thickness %
38 %%%%%%
39
40 d = 1000;
41
42
43 %%%%%%
44 % Calculations %
45 %%%%%%
46
47 r_012 = fresnel_am_tf_s(n_0,n_1,n_2,d,wavelength)
48
49 R_012 = r_012.*conj(r_012);
50
51 plot(x,y,'g',wavelength,R_012,'--k')
52 title(['{'Fresnel reflectance equation plotted on NanoCalc simulated reflectance ...
      'curve'}']])
53 xlabel('Wavelength (nm)')
54 ylabel('Reflectance (%)')
55 legend('Simulation','Fresnel')

```

```

1 clear all
2 close all
3
4
5 %%%%%%
6 % Air_Cauchy_SiOx_SI(100).xy %
7 %%%%%%
8
9 %%%%%%
10 % Load data %
11 %%%%%%

```

```

12
13 load Air_Cauchy_SiOx(2nm)_SI.xy
14
15 x = Air_Cauchy_SiOx_2nm_SI(:,1);
16 y = Air_Cauchy_SiOx_2nm_SI(:,2);
17
18 %%%%%%%%%%%%%%
19 % Physics %
20 %%%%%%%%%%%%%%
21
22 wavelength = [400:1041];
23
24 %%%%%%%%%%%%%%
25 % Refractive index %
26 %%%%%%%%%%%%%%
27
28
29 n_0 = 1;
30
31 A = 1.4450;
32 B = 3e4;
33 C = 4e7;
34 n_1 = cauchy(wavelength,A,B,C);
35
36 load dispersion_SiOx.dat
37 disp1 = dispersion_SiOx(251:1:892,:);
38 n_2 = transpose(disp1(:,2))-li.*transpose(disp1(:,3));
39
40 load dispersion_Si(100).dat
41 disp2 = dispersion_Si_100_(251:1:892,:);
42 n_3 = transpose(disp2(:,2))-li.*transpose(disp2(:,3));
43
44 %%%%%%%%%%%%%%
45 % Thickness %
46 %%%%%%%%%%%%%%
47
48 d1 = 1000;
49 d2 = 2;
50
51 %%%%%%%%%%%%%%
52 % Calculations %
53 %%%%%%%%%%%%%%
54
55 r_0123 = fresnel_am_tf_lay_sub(n_0,n_1,n_2,n_3,d1,d2,wavelength);
56
57 R_0123 = r_0123.*conj(r_0123);
58
59 plot(x,y,'g',wavelength,R_0123,'--k')
60 title({'Fresnel reflectance equation plotted on NanoCalc simulated reflectance ...',
        'curve'})]
61 xlabel('Wavelength(nm)')
62 ylabel('Reflectance(%)')
63 legend('Simulation','Fresnel')
```

## B.4 Solvent vapour annealing ambient study

```

1 clear all
2 close all
3
4 tic
5
6 %%%%%%
7 % Physics %
8 %%%%%%
9
10 wavelength = (450:900);
11
12 air = [1:0.1:2]; %Defining Refractive index limits.
13
14 framevalues = []; %Define empty array where all data will be saved.
15
16 %%%%%%
17 % Load data %
18 %%%%%%
19
20 load ambientinvestreflectance
21
22
23 %%%%%%
24 % Loop %
25 %%%%%%
26
27 it = length(ambientinvestreflectance(:,1));
28
29 % For loop for fitting each SVA measurement.
30 for z = 1:it
31
32 y = ambientinvestreflectance(z,:);
33
34 MSE = []; %Define empty array to save data for one full SVA Measurement.
35
36 %%%%%%
37 % Reflective Index %
38 %%%%%%
39
40
41 % For loop for fitting refractive index of Air.
42 for k = 1:length(air)
43
44 list = [];
45
46 n_0 = air(k);
47
48
49
50
51 load dispersion_SiOx.dat

```

```

52     disp_2 = dispersion_SiOx(301:1:751,:);
53     n_1 = transpose(disp_2(:,2)) -li.*transpose(disp_2(:,3));
54
55     load dispersion_Si(100).dat
56     disp_3 = dispersion_Si_100_(301:1:751,:);
57     n_2 = transpose(disp_3(:,2)) -li.*transpose(disp_3(:,3));
58
59
60 %%%%%%%%%%%%%%
61 % Thickness %
62 %%%%%%%%%%%%%%
63
64     d_1 = 2;
65
66 %%%%%%%%%%%%%%
67 % Reflectance Calculations %
68 %%%%%%%%%%%%%%
69
70     r_01 = fresnel_am_tf_s(n_0,n_1,n_2,d_1,wavelength);
71
72     R_01 = r_01.*conj(r_01);
73
74
75 %%%%%%
76 % MSE %
77 %%%%%%
78
79     Δy = y - R_01;
80     sqΔy = Δy.^2;
81     sumsq = sum(sqΔy)./length(wavelength);
82
83
84     list = [air(k),sumsq];
85     MSE = vertcat(MSE,list);
86
87     end
88
89 [row,column] = find(MSE==min(min(MSE(:,2))));
90 tempvalue = MSE(row,:);
91
92 framevalues = vertcat(framevalues,tempvalue);
93
94 end
95
96 %save('frame_val.mat','framevalues') %Saving to file
97
98 toc

```

```

1 clear all
2 close all
3
4 %%%%%%%%%%%%%%
5 % Load Data %

```

```

6 %%%%%%%%
7
8 load ambientinvestreflectance
9 load frame_val.mat
10
11 %%%%%%%%
12 % Physics %
13 %%%%%%%%
14
15 wavelength = (450:900);
16
17 %%%%%%%%
18 % Plotting %
19 %%%%%%%%
20
21 figure('units','normalized','outerposition',[0 0 1 1])
22 plot((12:length(ambientinvestreflectance(:,1))).*10,
23 framevalues(12:length(ambientinvestreflectance(:,1)),1))
24 axis([0 11000 1 1.4])
25 title('Solvent vapour annealing ambient study')
26 xlabel('Seconds')
27 ylabel('Refractive Index')
28 yticks([1 1.1 1.2 1.3 ])
29 legend('Refractive index of Ambient')
30 hold on
31 line1 = vline([1000 2000 3000 4000 5500 6500 7500 8500 ...
    9500],{'k:','k:','k:','r:','r:','k:','k:','k:'},{'','','','Max ...
    swelling','','','',''} );
32 hold off
33
34
35 figure('units','normalized','outerposition',[0 0 1 1])
36 plot((12:length(ambientinvestreflectance(:,1))).*10,
37 framevalues(12:length(ambientinvestreflectance(:,1)),2).*length(wavelength), 'k.')
38 axis([0 11000 0 0.3])
39 title('Solvent vapour annealing ambient study - MSE')
40 xlabel('Seconds')
41 ylabel('MSE')
42 hold on
43 line1 = vline([1000 2000 3000 4000 5500 6500 7500 8500 ...
    9500],{'k:','k:','k:','r:','r:','k:','k:','k:'},{'','','','Max ...
    swelling','','','',''} );
44 hold off

```